THEORETICAL UV-VIS SPECTROSCOPY AND MOLECULAR SIMULATIONS ON DOPED POLYANILINE AS A HYDRAZINE SENSOR

FATIN NADZIRAH SABRI

FACULTY OF SCIENCE
UNIVERSITY OF MALAYA
KUALA LUMPUR

2018

THEORETICAL UV-VIS SPECTROSCOPY AND MOLECULAR SIMULATIONS ON DOPED POLYANILINE AS A HYDRAZINE SENSOR

FATIN NADZIRAH SABRI

DISSERTATION SUBMITTED IN FULFILMENT OF THE REQUIREMENTS FOR THE DEGREE OF MASTER OF SCIENCE

DEPARTMENT OF CHEMISTRY
FACULTY OF SCIENCE
UNIVERSITY OF MALAYA
KUALA LUMPUR

2018

UNIVERSITY OF MALAYA

ORIGINAL LITERARY WORK DECLARATION

Name of Candidate: Fatin Nadzirah Binti Sabri

Registration/Matric No: SGR140019

Name of Degree: Master of Science (Except Mathematics & Science Philosophy)

Title of Thesis: Theoretical UV-VIS Spectroscopy And Molecular Simulations On Doped Polyaniline As A Hydrazine Sensor

Field of Study: Theoretical and Computational Chemistry

I do solemnly and sincerely declare that:

(1) I am the sole author/writer of this Work;
(2) This Work is original;
(3) Any use of any work in which copyright exists was done by way of fair dealing and for permitted purposes and any excerpt or extract from, or reference to or reproduction of any copyright work has been disclosed expressly and sufficiently and the title of the Work and its authorship have been acknowledged in this Work;
(4) I do not have any actual knowledge nor do I ought reasonably to know that the making of this work constitutes an infringement of any copyright work;
(5) I hereby assign all and every rights in the copyright to this Work to the University of Malaya ("UM"), who henceforth shall be owner of the copyright in this Work and that any reproduction or use in any form or by any means whatsoever is prohibited without the written consent of UM having been first had and obtained;
(6) I am fully aware that if in the course of making this Work I have infringed any copyright whether intentionally or otherwise, I may be subject to legal action or any other action as may be determined by UM.

Candidate's Signature Date:

Subscribed and solemnly declared before,

Witness's Signature Date:

Name:

Designation:

[THEORETICAL UV-VIS SPECTROSCOPY AND MOLECULAR SIMULATIONS ON DOPED POLYANILINE AS A HYDRAZINE SENSOR]

ABSTRACT

Polyaniline (PANI) is one of the conducting polymers known to have a reasonably good conductivity, is easy to prepared, stable, affordable and manifests redox properties. It has received attention in comparison to other organic compounds through on-going research work performed either in its native state or functionalized form. Emeraldine base, (EB) is acknowledged as the most useful form of PANI due to its high stability at room temperature. Besides, EB can be doped to the emaraldine salt (ES) which is the conducting form of the polymer. As for this study, EB has been doped with anions called sodium dioctyl sulfosuccinate (AOT^-) to use as a hydrazine sensor and the detection of hydrazine is then observed by using ultraviolet-visible (UV-VIS) spectroscopy. In order to have an insight into the conductivity mechanism as well as its effect on the UV-VIS spectroscopy, a comprehensive study about the molecular and electronic properties of different degrees of polymerization have been explored using quantum mechanical calculations together with molecular dynamics simulation. Through our computational study, it had been found that dimer form of ES that is composed of 8 rings in ratio of 1:1 benzoid and quinoid shows the closest ES UV-VIS peak with experimentally observed result. On the other hand, semi-empirical AM1 and PM6 as well as DFT (B3LYP functional) show the most reliable UV-VIS absorption peak simulation using the dimer model in comparison with the experimental spectra. Then again, DFT with B3LYP calculations are the most reliable calculations, manifesting a consistent lambda peak reduction as more cations at the ES chain are reduced. This is observed during the dedoping process simulation conducted on tetramer and ES compared to the experimental results.

Keywords: Emeraldine salt; UV-visible spectra; quantum mechanics; DFT

[SPEKTROSKOPI UV-VIS TEORI DAN SIMULASI MOLEKUL PADA 'DOPED' POLYANILINE SEBAGAI SENSOR HIDRAZIN]

ABSTRAK

Polianalin adalah antara polimer konduktor secara umumnya memiliki tahap konduktiviti yang bagus, mudah disediakan, stabil, mampu milik dan mempunyai sifat-sifat redoks berbanding dengan kompoun organik yang lain. Oleh itu, polianilin telah menerima perhatian yang khusus dan kerja-kerja kaji selidik yang menyeluruh sama ada di dalam keadaan asli mahupun keadaan berfungsi. Emaraldin asas, telah diperakui sebagai bentuk polianilin yang paling berguna memandangkan ia mempunyai stabiliti yang tinggi pada suhu bilik. Selain itu, emeraldin asas juga boleh didopkan menjadi garam emeraldin iaitu polimer di dalam keadaan konduktor. Bagi kajian ini, emeraldin asas telah didopkan dengan anion yang dipanggil natrium dioctyl sulfusuccinate (AOT^-), dan membolehkan garam emeraldin berpotensi bertindak sebagai penderia hidrazin. Kaedah pengesanan hidrazin dilakukan melalui pemerhatian terhadap spektroskopi ultraviolet nampak. Demi mendapatkan pemahaman yang jelas mengenai mekanisme konduksi, kajian secara terperinci mengenai sifat-sifat molekul dan elektronik telah dijalankan keatas beberapa darjah pempolimeran yag berbeza menggunakan pengiraan mekanik kuantum bersama dengan simulasi dinamik molekul. Menerusi kajian pengkomputan yang mendalam yang telah dijalankan, garam emeraldin dimer yang terdiri daripada 8 gegelung benzenoid dan quinoid dilihat mempunyai keputusan ultra violet nampak paling mirip dengan keputusan yang diperoleh dari eksperimen yang dijalankan. Selain itu, semi-empirical; AM1, PM6 dan DFT B3LYP menunjukkan keputusan ultra violet nampak paling hampir dengan keputusan ultra violet nampak yang dilihat melalui eksperimen . Manakala, kaedah *Density Functional Theory*, (DFT) khususnya B3LYP didapati memberikan keputusan yang paling berpadanan, iaitu penurunan tetap puncak ultra violet

nampak apabila bilangan kation pada rantaian ES berkurangan, bagi simulasi proses '*dedoping*' jika dibandingkan dengan keputusan eksperimen.

Kata kunci: Garam emeraldin; ultra violet nampak; mekanik kuantum; DFT

ACKNOWLEDGEMENTS

First and above all, I praise God, the almighty for giving me this opportunity and granting me the capability to proceed successfully. This thesis appears in its present form due to the assistance and guidance of several people. I would therefore like to offer my sincere appreciation to all of them.

Foremost, I would like to express my sincere gratitude to my supervisor Assoc. Prof. Dr. Vannajan Sanghiran Lee for the continuous support of my MSc study and research, for her patience, motivation, enthusiasm, and immense knowledge. Her guidance helped me throughout the research and writing of this thesis. I could not have imagined having a better supervisor and mentor for my MSc study.

I would also like to extend my sincere appreciation to Prof. Dr. Sharifuddin Md Zain, and Dr. Phang Sook Wai, for their valuable guidance. You have lead me working on my project with diverse exciting ideas and suggestions that eventually helped me to choose the right direction and successfully complete my thesis.

I will also like to take this opportunity to express my gratitude to my friends and family who supported me throughout the course of this computational chemistry project. I am thankful for their aspiring assistance, invaluably constructive criticism and friendly advice during the project. I am sincerely grateful to them for sharing their truthful and illuminating views on a number of issues related to the project.

I would also like to acknowledge Dr. Sim Yoke Leng of the Chemistry Department at University Tunku Abdul Rahman who checked this thesis, and I am gratefully indebted for her very valuable comments on this thesis.

TABLE OF CONTENTS

LIST OF FIGURES

LIST OF TABLES

LIST OF SYMBOLS AND ABBREVIATIONS

Δ	:	Delta
E	:	molar extinction
Σ	:	Sigma (Summation)
Ψ	:	Psi
2D	:	2 Dimension
3D	:	3 Dimension
A	:	Absorbance
AM1	:	Austin Model 1
AO	:	atomic orbitals
AOT^-	:	Sodium dioctyl sulfosuccinate
C	:	Concentration
CNDO	:	Complete Neglect of Differential Overlap
DFT	:	Density functional theory
EB	:	Emeraldine base
ECD	:	Electronic circular dichroism
E_{el}	:	Electronic energy
ES	:	Emaraldine salt
E_{tot}	:	Total energy
H	:	Hamiltonian operator
HOMO	:	Highest Occupied Molecular Orbital
$H_{\mu v}$	:	One electron core Hamiltonian
INDO	:	Intermediate Neglect of Differential Overlap
IR	:	Infrared
L	:	optical path length
LUMO	:	Lowest Unoccupied Molecular Orbital
MM	:	Molecular Mechanics

MMFF	:	Merk Molecular Force Field
MNDO	:	Modified Neglect of Differential Diatomic
MO	:	Molecular Orbitals
NDDO	:	Neglect of Differential Diatomic Overlap
ORD	:	Optical rotary dispersion
PES	:	Potential Energy Scan
PM3	:	Parametric Method 3
PM6	:	Parameterization Method 6
$P_{\lambda\sigma}$	:	Density Matrix
R	:	Coordinate of electron
ROA	:	Raman optical activity
TD-SCF	:	Time dependent self-consistent field
UFF	:	Universal Force Field
UV-VIS	:	Ultraviolet-isible
VCD	:	Vibrational circular dichroism
Vee	:	electron-electron interaction
V_{ext}	:	Interaction with the external potential
VWN	:	Vosko, Wilk, and Nusair
WHO	:	World Health Organization
ZDO	:	Zero Differential Overlap
Z_{α}	:	the charge of nucleus at $R_{\alpha.}$

LIST OF APPENDICES

CHAPTER 1: INTRODUCTION

1.1 Polymer

Polymers are macromolecules composed of repeated units of a small chemical unit or 'monomer'. The first part of the word 'monomer' comes from the Greek word 'mono' meaning 'single' and the second part comes from the Greek word 'mer' meaning 'part': the monomer is therefore a 'single part'. Whereas, the term 'poly' in Greek word means 'many' which then eventually made the meaning of 'polymer' is 'many parts' (Bovey & Wlnslow, 1979). For example, polytetrafluoroethylene (PTFE) is formed through polymerisation of tetrafluoroethylene monomer as indicated in the Figure 1:

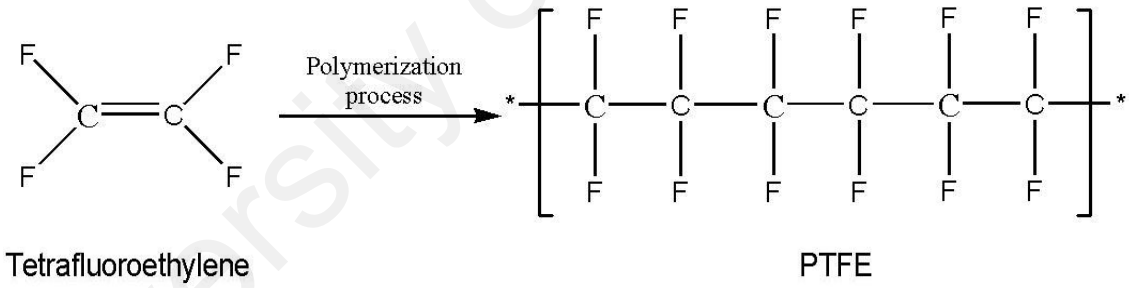

Figure 1.1: The formation of PTFE from tetrafluoroethylene monomer.

Certain polymers are found in nature, for example silk, proteins, and cellulose, whereas many others can only be produced synthetically. These includes polyethylene, nylon and polystyrene. However, there are also naturally occurring polymers that can be produced synthetically. Natural (Hevea) rubber which is known as polyisoprene in its synthetic form is one of the significant example (Fried, 2014).

Despite not realizing it, everyone is actually familiar with polymers. Nowadays, polymeric materials manufacturing is a major worldwide industry and we use them in almost all areas of daily life. For different polymeric materials, properties of a given type are often immensely different and this is sometimes true even for the same material in different physical states. Therefore, they can be said to be an astonishingly versatile class of materials.

In general, polymers are well known for their advantage that is economical due to the cheap price of monomers, can be produced in large amounts, anti-corrosion along with being light in weight. Typically, polymer is used in the production of plastic-based or rubber-based applications such as mineral water bottle, food container and tyre on top of being used for insulation purpose. However, the insulating properties of polymers set limitations to advanced applications that mostly requires the material to be conductive in nature.

1.2 Conducting Polymers

In 2000, Nobel Prize in Chemistry was awarded to Alan G. MacDiarmid, Hideki Shirakawa and Alan J. Heeger for the invention of conductive polymer, polyacetylene, that they made in the 1970s. Their discovery has changed the perception of the world on polymers which were previously recognized as insulators and having opposite properties of that of metals. The new conducting polymer has broadened the application of the conventional polymer that only offers significant resistance to electrical conductions (Peter & Durga, 2012).

Electronically conducting polymers have processing advantages and mechanical parameters of polymeric materials while simultaneously possessing electronic properties of semiconductors. These great combinations allowed conducting polymers to receive great attention in academics and industries as a topic of investigation. Conjugated

structure of alternating single and double bonds is the key to the characterization of conducting polymers (Atassi, 2008). The unsaturated π-bonded polymers have large electron affinities as well as small ionization potentials which enable the system to be easily doped by either oxidation or reduction process. This is due to the fact that electron of π character can be easily added or removed to form polymeric ion (Bredas & Street, 1985).

The development of conductive polyacetylene made conducting polymers to gain remarkable attention, which resulted in the invention of conductive polythiopene, polypyrrole, polyaniline and various conducting polymers. The unique properties of conducting polymers are low density, flexibility of design, and ease of fabrication, on top of being low cost. These generally give them advantage over other materials. Today, conductive polymers have been used in many aspect of life, for example, compact capacitor, electromagnetic shielding of computer, solar cells, light-emitting diodes and many more.

1.3 Polyaniline (PANI)

Among all conducting polymers, PANI is the most important conducting polymer due to its easy preparation, good processing properties and environmental stability (Nascimento et al., 2007). It is a semi-flexible rod polymer that can be converted to conductive polymer by appropriate oxidation or doping. The unusual electronic properties such as electrical conductivity, high electron affinity, low energy optical transitions, and low ionization potential are due to the π-electron backbone contained in PANI.

In general, PANI can exist in three different oxidation states which are leucoemeraldine (LE) which is a fully reduced form, half oxidised emeraldine base (EB) as well as fully oxidised form known as pernigraniline (PE) as shown in Figure 1.2. Among these three basic oxidation states, EB is acknowledged as the most useful form of

PANI due to its high stability at room temperature. Emeraldine salt (ES) form of PANI has a mixed oxidation state of reduced benzoid unit and oxidized quinoid units.

The ability of PANI to function as a conductor by protonation of non-conductive EB leading to conductive (ES) has been disclosed by MacDiarmid and co-workers in the mid-1980s (Chiang & MacDiarmid, 1986). Enhancement of electrical conductivity by several orders of magnitude was observed in ES by the doping process (Kavirajaa et al., 2014). Upon protonation with an acid, the resulting ES form of polyaniline is highly electrically conducting and poses high stability at room temperature. On the other hands, LE and PE are poor conductors, even when protonated with an acid (Alvarez & Sordo, 2008).

Generally, conductivity is influenced by a variety of factors including the polaron length, the conjugation length, overall chain length and by the charge transfer to adjacent molecules (Ravichandran & Baldwin, 1983). The remarkable conducting properties that PANI shows have received much attention in sensor application either in its native state or functionalized form.

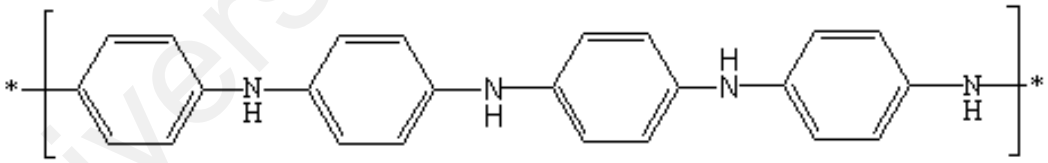

(a)

Figure 1.2: Three different oxidation states of PANI (a) leucoemeraldine (LE) (b) emeraldine base (EB) and (c) pernigraniline (PE).

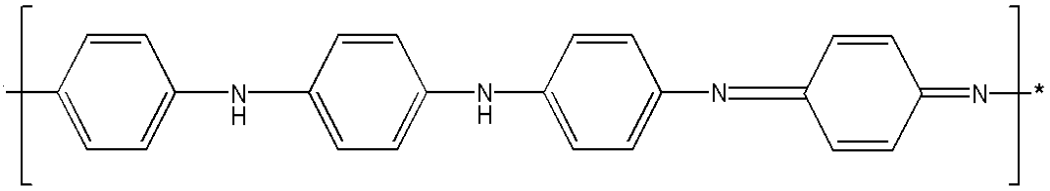

(b)

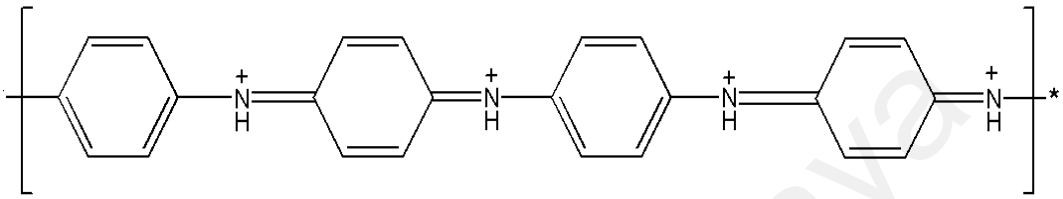

(c)

Figure 1.2, continued

1.4 Hydrazine Sensor

Hydrazine is an oily, colourless liquid that sometimes exist as a white crystalline compound (Choudhary & Hansen, 2012). Hydrazine is also known as diamine, nitrogen hydride, levoxine, and oxytreat 35 with a molecular formula of N_2H_4. Hydrazine is inflammable in the presence of open heat, sparks, flames and oxidizing materials. Above all, in the presence of oxidizing materials and metals hydrazine can be highly explosive. Besides, hydrazine is also incompatible with acids and moisture (Audrieth & Ogg, 1951). On the other hand, hydrazine is identified as a powerful reducing agent and a very highly reactive base. Hydrazine has a chemical structure as displayed in Figure 1.3:

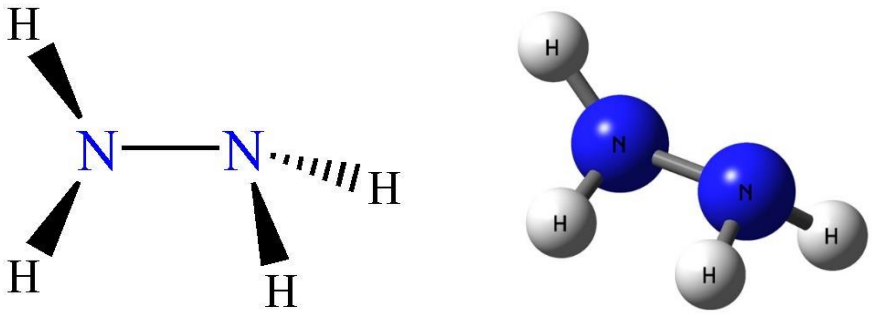

(a) (b)

Figure 1.3: The chemical structure of hydrazine (a) 2D structure (b) 3D structure.

Generally, hydrazine is used as a foaming agent in polymer foams preparation, on top of its role as a precursor to polymerization catalysts in pharmaceuticals industry. In addition, hydrazine is used in the preparation of the gas precursors used in air bags besides functioning as various rocket fuels. It is as an inhibitor to corrosion within both conventional electrical and nuclear power plant steam cycles. It is also used to control the pH and decrease the concentration of dissolved oxygen in water used in large industrial boilers as well as a propellant on board space means of transportation. Hydrazine is also useful in the elimination of halogens from wastewaters, nickel plating, and in the development of photograph (Choudhary & Hansen, 2012). Basically, hydrazine has various applications which lead to the possibility that they may be discharged into the environment with concentrations above the maximum recommended level of 1 ppm.

The severe health impact of hydrazine made the detection of its presence important in different kind of samples such as environmental, water and industrial, important. Besides, adverse systemic health effects or cancer may in develop on people exposed to hydrazine. Hydrazine has been classified as a possible carcinogen by the World Health Organization (WHO), the International Agency for Research on Cancer and the U.S. Environmental Protection Agency (Choudhary & Hansen, 2012). Hence, there is a demand for designing

an economical, simple and accurate device for the determination of trace amounts of hydrazine in any sample.

The instrument that is frequently used to sense and react to any type of input from physical or chemical environments is generally labeled as a sensor. The example of physical parameter or typically called inputs could be speed, motion, heat, light, pressure, humidity, or any one of other environmental occurrences. The yield or commonly called output is usually a signal that can be electrically measured and can be converted to human-readable display or additional information processing. To wisely choose the best sensor to give the most accurate result of our measurement, there are several features that needed to be taken into consideration including accuracy, measurement range, environmental condition for instance humidity or temperature, resolution of detection, and cost (Shieh et al., 2001).

One of the examples of sensor is a photosensor. A photosensor is used to detect the presence of infrared transmission (IR), visible light, and/or ultraviolet (UV) energy. Most photosensors have a property called photoconductivity due to the presence of semiconductor, in which the intensity of radiation striking the material determines the electrical conductance.

In 2014, Kavirajaa and co-worker have conducted a research of using a doped PANI as a hydrazine sensor. As a result, they have developed a chemical sensor that is capable of detecting the presence of hydrazine by monitoring it through UV-VIS spectra.

1.5 Ultraviolet-Visible Spectra

One of the oldest methods in molecular spectra is called the Ultraviolet (UV)-Visible (VIS) spectra. At an early date, precisely 1852, the definitive formulation of the Bouguer-Lambert Beer Law formed the basis for the quantitative evaluation of absorption

measurements (Grinter & Threlfall, 1992). Based on the Beer-Lambert Law or also known as Beer's Law, the concentration, c of the substance in solution is proportional to the absorbance, A and also the optical path length, l, for example the dimension of the cell or cuvette. Thus, UV-VIS spectra can also be used to measure the concentration of a sample. The Beer's Law can be conveyed as the following equation;

$$\mathbf{A = \varepsilon cl} \qquad \textbf{(}1.51\textbf{)}$$

where, ε = molar extinction, which is constant for a particular substance at a particular wavelength ($dm^3\ mol^{-1}\ cm^{-1}$)

An absorption spectrum will display a number of absorption bands associated with structural groups within the molecule as different molecules absorb radiation of different wavelengths.

In both atoms and molecules, absorption of UV and VIS radiation correspond to the excitation of electrons, from lower to higher energy levels. However, only light with the specific amount of energy will cause excitation from one level to another will be absorbed since the energy levels of matter are quantized. The possible electronic transitions of electrons are as shown in Figure 1.4 ("Ultraviolet-Visible Spectra (UV)", 2009):

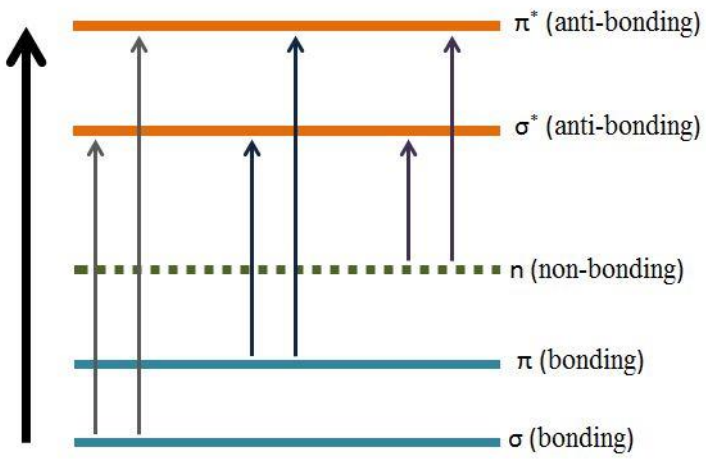

Figure 1.4: UV-VIS energy diagram (modified from "Ultraviolet-Visible Spectra (UV)", 2009).

An UV-VIS spectrum holds a significant value due to its varied applications in chemistry, biochemistry and physics. Recently, with the development of computational chemistry, UV-VIS spectrum can be predicted using quantum computations.

1.6 Quantum Mechanics Based Computational Approach

The development in computational sciences have made many aspects of research capable of being explored via computational approach. Materials science involving polymers is among the subject of interest.

Computational science is a rapidly developing multidisciplinary field involving computational chemistry, physics, biology and other sciences. Besides the theoretical and experimental aspects, computational science can be considered as the third way of doing science. With the usage of computers, one can now conduct tremendous complex simulations or calculations using mathematical methods that have been sufficiently well developed. It can be automated for implementation on a computer to elucidate problems in various scientific disciplines (David, 2001).

The field of study and research that involves the usage of computational methods to investigate or solve chemistry related problems or research questions is called computational chemistry. It is important to note that computational chemistry is also known as molecular modeling (Lewars, 2011). A variety of complicated questions in chemistry can be solved by computational methods due to the fact that chemists develop better algorithms for solving particularly difficult problems, or developing new ways to visualize or encode data, either as input to or output from a model along with the fact that computers are becoming more powerful and ubiquitously available (Christopher, 2004).

Over the past few decades, properties of molecules have been accurately predicted with the help of powerful molecular simulation and modeling tools that have been developed. These could be achieved largely due to the dramatic increase in computer speed and the design of efficient quantum chemical algorithms. It has been proven that computational chemistry is valuable in studying the properties of materials, for example in materials science. With the aid of computational chemistry, investigation on plastics, superconductors, semiconductors, ceramics have been conducted. Computational chemistry is known to be environmentally secure, it is cheaper, and it is also faster as compared to experiments. However, it cannot replace experiment, which remains the final judge of truth about nature. This is because, to invent something, be it new drugs or new materials, one still needs to go into the lab. Nonetheless, gradually, scientists in general are engaging it before proceeding with the experimental project, since computation has become so dependable in some aspects (Lewars, 2011).

1.7 Problem Statement

As previously mentioned, in 2014, Kavirajaa and colleagues have conducted the experimental work to design a chemical sensor for hydrazine detection by using a doped PANI. This has resulted in the invention of the hydrazine sensor that is capable of detecting the compound via UV-VIS spectra. However, they only covered the experimental work on that particular topic, thus, to widen the research in this particular topic of interest and explore more, computer aided simulations have been performed in this work to look for the most suitable methods that correlate well with the result produced in the experimental part.

1.8 Research Objectives

In order to find the most suitable computational method that correlates with the experimental work, this research has been conducted with the following objectives:

1. To build the molecular model and optimize the structure of ES-PANI with quantum chemical methods.
2. To calculate and characterize the UV-VIS spectrum of the structures of doped-aniline and hydrazine with quantum chemical methods.
3. To perform the simulation for de-doping process of polyaniline as hydrazine sensor.

CHAPTER 2: LITERATURE REVIEW

2.1 Computational study of PANI

Various studies have been conducted to explore the unique properties of polyaniline (PANI) that have enabled it to work as a conducting polymer. A unique solvatochromic and thermochromic properties displayed by PANI together with the attractive optical and structural properties have attracted researchers to carry out intense studies and research on this particular polymer including from a computational aspect.

In 2005, the doping of PANI by acid-base chemistry was studied by using Density Functional Theory (DFT) with periodic boundary condition and a 6-31g (d,p) basis set. The three functionals that have been employed are LSDA, PBE and PBEh. According to the results analysed using density of states, the PBEh calculation lead to spectroscopic simulation that came close to the available experimental data compared to the other two functionals. Generally, the fully optimised geometries of the studied structures, EB and ES, are consistent with those observed in MacDiamid and co-workers' mechanism. Likewise, the simulated dihedral angles among the different C_6 rings in those structures are consistent with the structural information provided by X-ray data. Furthermore, according to the computaed energies, bipolaronic lattice ES was found to be the most stable structure compared to others. Thus, it is responsible for the properties displayed by the proton-doped EB, in particular, its conductivity. Finally, PBEh density of state calculation indicated that the bipolaronic lattice ES is compatible with the optical transition at about 1.6, 2.2, and 4.1 eV, which in fact correlates well with the optical absorption spectra of protonated PANI that exhibit the peaks at 1.5, 2.8, and 4.1 eV (Varela-Alvarez et. al., 2005).

However, a further study of the ES structures found conflicting results to the previous study. In contrast, polaron lattice was found to be the most stable phase of doped PANI. This is the result of their work which is a step forward in comprehending the mechanism of formation of conducting polymer. The output of some important experimental results on doped PANI, specifically, it's magnetic behaviour, the existence of polaron-bipolaron equilibrium, and the "metallic island" model for the ES conducting purpose have been rationalized in terms of a trication polaron lattice based on periodic boundary condition PBEh/6-31g(d,p) calculations. The optical transition and the structural parameter predicted are analogous to the x-ray information and optical absorption data available for ES (Varela-Alvarez et. al., 2008).

In addition, other studies that has been performed to identify multiplicity of ES form of PANI, at the semi-empirical (AM1) and/or molecular mechanics (AMBER96) level, revealed that the multiplicity for the ground state ES cannot be specified due to the low and high-spin electron configuration of almost equal probabilities in both aqueous and vacuum media. However, the vacuum media stabilizes the high-spin state. The average torsional angle which is the most sensitive structural parameter depends on the presence of the solvents as well as the spin state of the components in the cluster. A comparison with the single chain showed that torsion angle decreases in singlet aggregates, but a contradictory result was seen in the high-spin ones. The effect of hydration was to flatten the singlet, mildly deforming the triplet and substantively twisting mixed structures. On the other hand, in all cases, hydration enhances counter ion separation besides strengthening the van der Waals interactions. In the 2 stack molecules model study, the stacks with the most attractive van der Waals interaction were the proper model but they gave rise to short wavelength transitions in the electronic spectra. Meanwhile, long wavelength lines were produced by the model that have the second best van der Waals interaction. Concurrently, the simulation of the electronic spectra show that the excitation

peak covers a compelling broad range from UV to Near Infrared (NIR) and Infrared (IR) regions. In particular, at about 800nm, there is low-spin cluster absorption whereas medium and high-spin aggregates have maxima at shorter wavelengths but then, this produces a large number of relatively intense absorptions (Zhekova et al., 2007).

2.2 Computational Chemistry Programs – The Gaussian suite of programs

One of the most widely used program for molecular modelling and simulation is the Gaussian suite of programs. Gaussian has been developed into several series which all are basically series of electronic structure programs. The latest version of the Gaussian is Gaussian 09. Gaussian 09 program offers vast applications which enable them to be used in various scientific fields such as chemistry, physic, biochemistry and chemical engineering. By implementing the elemental laws of quantum mechanics, there are various parameters that can be produced and predicted using Gaussian 09 such as:

- Molecular structures and energies
- Vibrational frequencies
- Energies and structure of transition states
- Molecular orbital
- Bond and reaction energies
- Atomic charges and electrostatic potentials
- IR and Raman Spectra
- Reaction pathway
- Hyperpolarizabilities and polarizabilities
- Thermochemical properties

Gaussian 09's models can be implemented to both stable compounds and species that are hard or impossible to be experimentally observed, for instance, transition structures

and short-lived intermediates. Computations of the models can be carried out on systems in their ground state or excited state, and in solution or in the gas phase (Foresman & Frisch, 1996). A comprehensive investigation on almost any chemical problems of interest can be carried out with Gaussian 09. As an example, not only the molecular structures can be minimized reliably and quickly, the program can also predict spectra. Variety of spectra can be predicted via Gaussian 09 which include UV-VIS, NMR, IR and Raman, Electronic circular dichroism (ECD), Raman optical activity (ROA), Vibrational circular dichroism (VCD), Optical rotary dispersion (ORD), Hyperfine spectra (microwave spectra), Herzberg-Teller, Franck-Condon and Franck-Condon/Herzberg-Teller analyses. Based on the results of several studies conducted, it can be said that Gaussian 09 has successfully computed relevant spectroscopic constants and related molecular properties with outstanding accuracy using suitable theoretical models ("Gaussian 09: Expanding the limits of computational chemistry", 2014).

Briefly, a method or theoretical model is a specific set of approximations implemented to model a system. The combinations of the approximations together with a computational algorithm are applied to atomic orbitals, defined by the basis set. Basically, the methods can be classified into 4 main types ranging from the less accurate to more accurate calculation as molecular mechanics, semi-empirical, ab initio and density functional method. The selection of the suitable theoretical model highly depends on the level of approximation and on the size of the system.

Ab initio method is a type of computation based on theoretical principles only, without using any experimental data. Even though the mathematical approximations used in the above mentioned methods are different, they do have the same basic approach. However, *ab initio* is the most popular type of model, despite the fact that the calculations are time consuming. Hartree-Fock (HF) approximations constitute the basic *ab initio* model.

Instead of considering explicit repulsion interactions, HF uses the approximation that Coulombic electron-electron repulsion can be averaged. There are two ways to compute atomic or molecular orbitals using HF which are RHF (restricted) or UHF (unrestricted). RHF is suitable method for species with paired electrons because it uses the same orbital spatial function for electrons in the same pair; thus, there is no spin contamination. UHF on the other hand uses a separate orbital for each electron, even if they are paired, thus, it is good to be used for ions, excited states, radicals, and etc. Nevertheless, the exclusion of electron correlation is recognized as the major drawback of HF method. In addition, Moller-Plesset perturbation theory which is denoted as MPn (n = 2,...,6) is another example of ab initio calculation method. Generally, MP2 and MP4 are the only methods used in practice, since the other n's are either do not significantly improve the results compared with a lower level of complexity or are computationally expensive. Meanwhile, Configuration Interaction (CI) method of calculation is mostly used for excited states. CI is well known for its accuracy but is very CPU extensive.

Semi-empirical method is a computational method that uses a certain number of experimental data during the calculation. For instance, a fixed value has been set for bond lengths of a specific type of molecules bonding, independently of the system (for instance, 134 pm will always be interpreted as C=C bond length). As a result, computational speed has been dramatically increased, but in general the results produced are not very accurate. Semi-empirical methods are commonly used for very big systems, due to the fact that they can handle large calculations. Zerner's Intermediate Neglect of Differential Overlap (ZINDO) is one of the examples of semi-empirical method (Zerner, 2001). It is typically used to compute UV transitions. This is because it is parameterized to reproduce electronic spectra. Another semi-empirical method example is the Austin Model 1 (AM1). AM1 is a method that is often used to model organic molecules.

The Density Functional Theory (DFT) method, which is another quantum based method, is becoming more and more prevalent basically due to the time needed for the complete computation is significantly less, yet, the results obtained are as good as the ones computed using *ab initio* methods. The difference between DFT and HF calculations is that the parameters used to compute the energy. DFT method uses the electron density to compute energy instead of a wave function. B3LYP is the most widely used DFT functional. B3LYP corrects for both gradient and exchange correlations, thus, for that reason this method is called a hybrid functional. Meanwhile, another DFT functional which is PW91 is a Gradient-corrected method.

The suitable computational method for bigger molecules or systems is molecular mechanics (MM). MM methods approximate bonds as springs and atoms as spheres. Instead of using wave function or electron density for the energy calculation, they use an algebraic equation. The constants used in the algorithm are obtained from other calculations or experimental data that is stored in a data library. The combination of constants and algorithm is known as a force field. Universal Force Field (UFF) is one of the popular methods and can be applied on both organic and inorganic molecules. Merck Molecular Force Field (MMFF) is another general-purpose model, which is applied generally for organic systems (Tomberg, 2013).

It is important to note that besides the stated examples for each method, there are in fact many models for each method that offers distinct and unique advantages. Gaussian 09 offer the most advanced modeling capabilities available today, which significantly broaden the range of problems and systems that can be investigated. With Gaussian 09, more complicated problems and larger systems can be solved even on mediocre computer hardware ("Gaussian 09: Expanding the limits of computational chemistry", 2014). The selected methods for this study are explained in the following sections.

2.3 Density Functional Theory

Among computational methods available, Density Functional Theory (DFT) is the most popular method. This is because of the reliable results obtained with respect to the time consumed for the calculations along with the computational cost. DFT is able to achieve those advantages by including some of the effects of electron correlation that is much cheaper than traditional correlated methods.

In brief, Density Functional Theory (DFT) is a very effective approach to calculate the ground state properties of many-electron systems from first principles, in other words, it is a method of attaining an approximate solution to the Schrodinger equation of a many-body system. This method has been developed because it is impossible to solve the Schrodinger equation for a N-body system. If it is a simple 2D square potential case, or even hydrogen atom, the Schrodinger equation can be exactly solved to get the wave function of the system. Thus, in order to solve this problem, several approximations have been generated.

The first step in DFT is to reduce the number of degrees of freedom of a molecule. This step is accomplished using the so called "Born-Oppenheimer approximation" which is the most basic approximation. Since the forces on both the electrons and atomic nuclei are of the same order of magnitude, their momenta are also comparable. However, since the atomic nuclei are so massive in comparison to the electrons, which in fact, an electron has less than 1800 times the mass of each proton or neutron in a nucleus. Consequently, this makes electrons respond much more rapidly to changes in their surroundings than a nuclei can. These enable us to split our physical question into two pieces. For immobilised positions of the atomic nuclei, we solve the equations that describe the motion of electron. There is a lowest energy state, or configuration, of the electrons observed in a given set of electrons moving in the field of a set of nuclei (Sholl & Steckel, 2009). This lowest energy state is also called the ground state of the electrons, and the

parting of the electrons and nuclei into distinct mathematical problems is known as the Born–Oppenheimer approximation which described as time independent and non-relativistic as indicated in the equation:

$$\hat{H}\psi(r_1, r_2, \dots r_N) = E\psi\,(r_1, r_2, \dots r_N) \tag{2.21}$$

Precisely, the Hamiltonian operator, H, consists of a sum of three terms; the interaction with the external potential (V_{ext}), the electron-electron interaction (V_{ee}) and the kinetic energy. This can be written into a mathematical equation as:

$$\hat{H} = -\frac{1}{2}\sum_{i}^{N} \nabla_i^2 + \hat{V}_{ext} + \sum_{i<j}^{N} \frac{1}{|r_i - r_{j|}} \tag{2.22}$$

However, in materials simulation, the interaction of the electrons with the atomic nuclei is the only external potential that is of interest, which is:

$$\hat{V}_{ext} = -\sum_{\alpha}^{N_{at}} \frac{Z_\alpha}{|r_i - R_\alpha|} \tag{2.23}$$

Where;

r_i is the coordinate of electron i

Z_α is the charge of nucleus at $R_{\alpha.}$

Spin coordinate is neglected in order to focus the discussion only on the main features of DFT as well as to simplify the notation. Equation (2.21) is solved for a set of Ψ subject to the limitation that the Ψ are anti-symmetric. The ground state energy is signified by the lowest energy eigenvalue, E_0, and $|\Psi_0|^2$ is said to be the probability density of finding an electron with any particular set of coordinates $\{\mathbf{r}i\}$ (Harrison, 2003). The main feature of DFT is that the energy can be obtained directly from the electron density.

Functionals that are used in DFT computational methods can be divided into two categories which are traditional functional and also hybrid functional. Even under the traditional functional category itself, there are a various othe functionals that have been stipulated, commonly differentiated by the way that they treat the exchange and correlation components. Correlation and local exchange functionals include only the values of the electron spin densities. The popular local exchange functionals are Xα and Slater, while the most used local correlation functional is the local spin density treatment of Vosko, Wilk, and Nusair (VWN). On the other hand, Gradient-corrected functional encompasses both the values of the electron spin densities and their gradients. Sometimes, in the literature, such functional are also known as *non-local*. In 1988, Becke proposed this well-known gradient-corrected exchange functional. A widely-used gradient-corrected correlation functional is the LYP functional of Lee, Yang and Parr (Lewars, 2011). The famous B-LYP method is actually the combination of the mentioned functionals.

In addition, there are also a few hybrid functionals, which define the exchange functional as a linear combination of local, gradient-corrected exchange and Hartree-Fock terms. The exchange functionals were then further combined with a gradient-corrected and/or local functional. The well-known hybrid functionals is Becke's three-parameter formulation, which is available in the Gaussian program via the keywords B3LYP and

B3PW91. Becke-style hybrid functionals have been proven to be superior compared to the traditional functional defined so far.

Nowadays, the application of DFT calculations have promptly become a "standard tool" for various material modeling problems in diverse field of research including chemistry, materials science, physics, and multiple branches of engineering. To further emphasize on its application, DFT computational codes involve electronic, structural and magnetic properties studies of molecules, materials and defects. However, besides DFT, there are various other computational methodologies that uses variety of different algorithms that could be explored to find the most compatible result with the experimental provided data.

2.4 Semi-empirical Quantum Mechanics

Semi-empirical quantum chemistry method is another available computational methodology. Semi-empirical quantum chemistry methods are based on the ab initio formalism however it uses some experimentally derived empirical parameters such as dipole moments of molecules, or ionization energies of atoms. In order to accelerate calculations, the semi-empirical methods of quantum chemistry introduce rather drastic approximation after starting out with the ab initio formalism. It is important to note that the typical approximations made are by neglecting many of the less important terms in the ab initio equations. In addition, empirical parameters are assimilated into the formalism and calibrated against reliable theoretical reference or experimental data in order to compensate for the error produced by the assumptions. They are very important in computational chemistry in order to improve performances by addressing two limitations, specifically slow speed and low accuracy, besides, to treat large molecules with the full Hartree–Fock method without the approximations being too computationally expensive (Thiel, 2005).

The older method of semi-empirical uses simpler integral schemes such as Complete Neglect of Differential Overlap (CNDO) and Intermediate Neglect of Differential Overlap (INDO). On the other hand, modern semi-empirical models such as modified neglect of differential diatomic (MNDO), Austin Model 1 (AM1) and Parametric Method 3 (PM3) are all based on the Neglect of Differential Diatomic Overlap (NDDO) integral approximation. NDDO method is a method where the unit matrix is replaced with the overlap matrix S. This enable the replacement of the Hartree-Fock secular equation |H-ES| = 0 with a simpler equation that is, |H-E| = 0. Among all, NDDO is regarded as the best of these approximations as it retains higher multipoles of charge distributions in the two-center interactions, in contrast to CNDO and INDO that shortens the charge distribution after the monopole. However, all the different methodologies are categorised to the same class that is Zero Differential Overlap (ZDO) methods. ZDO is an approach involving the negligence of the insignificant electron repulsion integrals which are used in several approximate self-consistent field of molecular orbital schemes. In another words, all the products of atomic orbitals $X_\mu X_\nu$ are set to zero for μ, ν on different atoms. The ZDO approximation greatly simplifies the computation of wavefunctions by neglecting three- and four- center 2-electron integrals. Several parameterized corrections are made in order to correct for the approximate quantum mechanical model (Kahn, 2006).

Austin Model 1 (AM1)

AM1 is among the most used methods of semiempirical approach. AM1 is a semi-empirical method for the quantum calculation of molecular electronic structure that is based on the NDDO integral approximation. It is in fact a generalization of the MNDO approximation. MNDO is a valence-electron self-consistent field (SCF) MO treatment that applies the NDDO integral approximation together with a minimal basis of atomic

orbitals (AOs, ϕ_μ). The solution of the secular equations ($S_{\mu\nu}=\delta_{\mu\nu}$ for NDDO) yields the MO ψ_i and the corresponding orbital energies ε_i (Thiel, 2000).

$$\psi i = \sum_{\mu} C_{\mu i}\, \phi_{\mu} \tag{2.31}$$

$$0 = \sum_{\upsilon}^{\mu} (F_{\mu\upsilon} - \delta_{\mu\upsilon}\, \mathcal{E}_i)\, C_{\upsilon i} \tag{2.32}$$

Atomic orbitals (AO) are assigned using superscripts denoted with index μ, λ, σ, υ to an atom A or B, thus, the NDDO Fock matrix elements $F_{\mu\upsilon}$ form are as the following:

$$F_{\mu^{\mathrm{A}}\upsilon^{\mathrm{A}}} = H_{\mu^{\mathrm{A}}\upsilon^{\mathrm{A}}} + \sum_{\lambda^{\mathrm{A}}}\sum_{\sigma^{\mathrm{A}}} P_{\lambda^{\mathrm{A}}\sigma^{\mathrm{A}}} \left[(\mu^{\mathrm{A}}\upsilon^{\mathrm{A}}, \lambda^{\mathrm{A}}\sigma^{\mathrm{A}}) - \frac{1}{2}(\mu^{\mathrm{A}}\lambda^{\mathrm{A}}, \upsilon^{\mathrm{A}}\sigma^{\mathrm{A}})\right] + \sum_{\mathrm{B}}\sum_{\lambda^{\mathrm{B}}}\sum_{\sigma^{\mathrm{B}}} P_{\lambda^{\mathrm{B}}\sigma^{\mathrm{B}}}\ (\mu^{\mathrm{A}}\upsilon^{\mathrm{A}}, \lambda^{\mathrm{B}}\sigma^{\mathrm{B}}) \tag{2.33}$$

$$F_{\mu^{\mathrm{A}}\upsilon^{\mathrm{B}}} = H_{\mu^{\mathrm{A}}\upsilon^{\mathrm{B}}} - \frac{1}{2}\sum_{\lambda^{\mathrm{A}}}\sum_{\sigma^{\mathrm{A}}} P_{\lambda^{\mathrm{A}}\sigma^{\mathrm{B}}}\ (\mu^{\mathrm{A}}\lambda^{\mathrm{A}}, \upsilon^{\mathrm{B}}\sigma^{\mathrm{B}}) \tag{2.34}$$

Notice that $H_{\mu\nu}$ and $P_{\lambda\sigma}$ are elements of the one-electron core Hamiltonian and the density matrix respectively and (μν, λσ) indicate a two-electron integral. The summation of the repulsions E_{AB}^{core} and the electronic energy E_{el} between the core of all atoms A and B produce the total energy E_{tot} of a molecule.

$$E_{el} = \frac{1}{2}\sum_{\mu}\sum_{\upsilon} P_{\mu\upsilon}\ \left(H_{\mu\upsilon} + F_{\mu\upsilon}\right) \tag{2.35}$$

$$E_{tot} = E_{el} + \sum_{A<} \sum_{B} E_{AB}^{core} \quad (2.36)$$

The equations (2.31) - (2.36) reveals that MNDO models include only one-center and two-center terms that are responsible for most of its computational efficiency.

AM1 was published in 1985 after its development by Michael Dewar and co-workers. AM1 applied a modified expression for nuclear-nuclear core repulsion yet takes a similar approach to MNDO in estimating two-electron integrals. The off-centre attractive and repulsive Gaussian functions were added to nuclear-nuclear core repulsion terms in the MNDO expressions in order to improvise it. This lead to non-physical attractive forces that mimic van der Waals interactions. The modification also imposed reparameterization of the model, which was implemented with a specific attention on geometries of molecules, ionization potentials, and dipole moments. It is important to note that as the number of parameters per atom increased from 7 in MNDO to 13-16 per atom in AM1, the complexity of the parameterization problem also increased in AM1.The output of AM1 calculations are occasionally used as the parameterizations starting points of force fields in molecular modelling (Kahn, 2006).

Parameterization Method 6 (PM6)

The recent semi-empirical method that has been developed is known as Parameterization Method 6**, (**PM6). PM6 follows the tradition of other "Dewar-style" NDDO methods such as MNDO, AM1, PM3, SAM1, and PM5, but, has a difference in the core-core interactions, *d*-orbital on main-group elements, unpolarizable core, individual core-core corrections, and nitrogen sp2 pyramidalization. A more comprehensive parameter optimization then can be gained, which has, in turn, allowed about 70 elements to be parameterized. In addition, remarkable improvements have been made in the geometries prediction along with the correction of some long-standing faults

in PM3 and AM1. One of the significant examples is the almost total nonexistence of a hydrogen bond. This exact fault basically prohibited MNDO being used in modeling biochemistry since hydrogen bonding is crucial.

To further emphasize, four specific types of reference data that been used to parameterize all the former NDDO methods were dipole moments, ionization potentials, ΔHf, and molecular geometries. However, during the development of PM6, other types of reference data were found to be essential to be used. These new data are best regarded as"rule" due to their behavior. In this perspective, a rule can eventually be described as reference information that is a function of one or more other data.

These methods are not particularly accurate in comparison to the spectrum of ab-initio methods. In fact, many methods along with post-Hartree-Fock corrections and also larger basis sets are more reliable. However, the PM6 methods have advantages such as practicality, robust, and most importantly that it allows multiple systems to be modeled in an equitable amount of time, which is a condition that could not be accomplished with the more sophisticated ab-initio methods. Whilst slightly highlighting biochemical systems in parameterization, PM6 is a general purpose model of decent quality and the development of this new method is the contribution of James JP Stewart. (Stewart, 2007)

2.5 Highest Occupied Molecular Orbital (HOMO) and Lowest Unoccupied Molecular Orbital (LUMO)

Molecular Orbital (MO) theory has been proved to be a captivating part of chemistry due to its ability to give a remarkable insight into chemical reactions by analysing interaction between orbitals which consequently control the product that will be formed. Basically, chemist uses MO theory to illustrate the disposition of electrons in chemical structures. Molecular orbital theory has reinforced numerous physical methods and has provided evidence that the interpretations from molecular orbital theory do have some

experimental basis. Some examples of deduction that could be explained via molecular orbital theory are bond lengths, the energies of conjugated systems, and energy barriers to rotation. In addition, polarographic reduction potentials which are usually used to measure electron affinities seem to reasonably relate with the calculated energies of the conjugated systems of LUMO. On the other hand, there are quite a few ways that MO can be used to measure ionization potentials, and the results adequately correlated with the energies of the HOMO of conjugated systems (Fleming, 2010). Additionally, based on MO theory, the electrons are said to be delocalized which means that they are spread out all over the molecule. As a result, bonds in the molecules are considered to have electrons shared between nuclei. In 1981, Fukui and Hoffmann have been rewarded with Nobel Prize for the development of these ideas. Molecular orbital theory is important in ascertaining certain phenomena which may be used to explain chemical behavior. For example, the **h**ighest energy **o**ccupied **m**olecular **o**rbital (HOMO) of one molecule and the **l**owest energy **u**noccupied **m**olecular **o**rbital (LUMO) of the other molecule are acknowledge as the most significant orbitals in determining molecules reactivity and commonly known as *frontier* orbitals, because they lie at the outermost boundaries of the electrons of the molecules. Based on the perturbation theory, the larger the contribution of the orbital pair to the stabilization of an interacting system could be achieved by smaller level of separation of these two overlapping orbitals (Malmström, 1992).

Hoffmann and Woodward revealed that the stereo selection rules could be accounted for by observing the frontier molecular orbitals interaction. Furthermore, for any two new orbitals to be formed either by two atomic or molecular orbitals interactions, these five basic rules of the MO Theory need to be obeyed:

- The number of atomic orbitals assimilate is equivalent to the number of molecular orbitals.
- Electrons need to fill in the lowest energy orbital available.

- Following Pauli Exclusion Principle, the maximum number of electrons allowed in an orbital is 2.
- Referring to Hund's Rule, electrons only pair up after they have been spread out.
- One of the two MO's is a bonding orbital (lower energy) while the other one is an anti-bonding orbital (higher energy).

As displayed in Figure 2.1, the frontier orbitals interaction is illustrated as a HOMO-LUMO interaction:

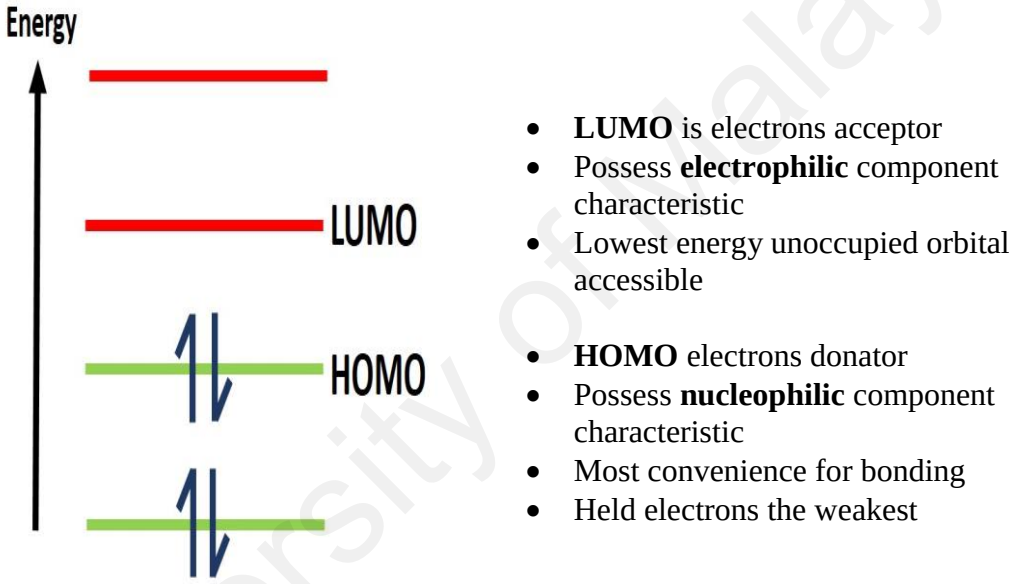

Figure 2.1: The HOMO-LUMO energy level diagram.

CHAPTER 3: METHODOLOGY

3.1 Molecular Models

PANI is a polymer consisting of the repeating unit of C_6H_4-N where nitrogen could occur as either amine (benzoid) or imine (quinoid) form as shown in Figure 3.1. Based on Figure 3.1, when n = 2, m = 0, PANI exists in a fully reduced state called Leucoemeraldine (LE). The fully oxidized state has imine links instead of amine links with n = 0, and m = 2 and known as Pernigraniline (PE) (Figure 1.2). The Emiraldine base (EB) exists in the condition of n = m = 1 where Emiraldine salt (ES) is a doped (protonated) EB, with the imine nitrogens protonated by an acid. Through protonation, the diiminoquinone-diaminobenzene state can be delocalized. The ES polaron model as in Figure 3.1(b) was built without the presence of dopant (AOT^-). Conformational search for the torsion angle of monomer and dimer model between the two rings as shown in Figure 3.2 were performed. The four different degrees of polymerization in which n = 1, 2, 3 and 4 were explored where the UV spectra were compared.

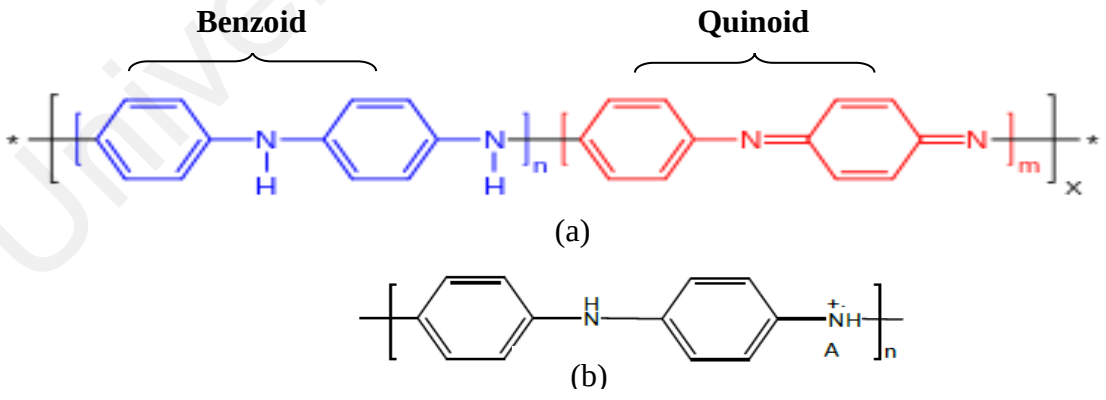

Figure 3.1: (a) Basic structure of polyaniline where n = m = 1 to 4 and degree of polymerization (x) = (n+m)/2 and (b) Structure of ES in polaron lattice form.

3.2 Quantum mechanical (QM) calculations

All calculations were performed by using quantum mechanical package Gaussian 09 (Version 09; Frisch, 2009). In order to get the most stable structure of ES, a systematic conformational search had been conducted with semi-empirical method, AM1, to observe the conformations between all the connected rings for monomer, dimer, trimer and tetramer model. Example of the torsion angle scan is as illustrated in Figure 3.2.

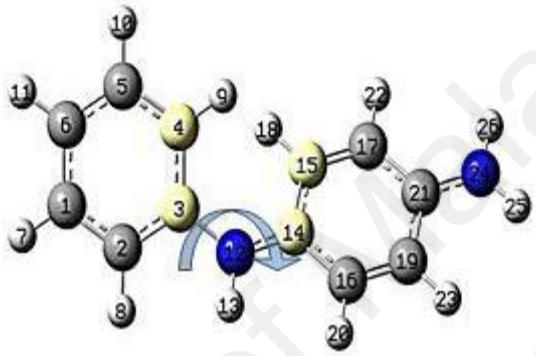

Figure 3.2: The scan torsional angles for monomer ES (torsion: 4, 3, 14, and 15) with step size of 30° using AM1 method for the conformational search.

A step size of 30 torsional angles was employed and 4 best conformations were finally generated in each case. The Potential Energy Scan (PES) as well as the superimposed process have also been conducted on the dimer ES for further confirmation of the lowest energy geometries. The geometric structures of the unit based conjugated segments with numbers of repeated monomers n = 1, 2, 3 and 4 were further optimized using the density functional theory (DFT) with the B3LYP functional and the 6-31g (d,p) basis set. For electronic spectral calculation, single point energy calculations were conducted using time dependent self-consistent field approach, TD-SCF. Several methods of calculations such as AM1, PM6, B3LYP, CAM-B3LYP, LSDA MO62X and PBEPBE have been explored to search for the most accurate method to be used for further calculations. Amongst all methods, DFT, AM1 and PM6 was adopted to be used for further calculation

due to the fact that they show better accuracy and more reliable results for the polymer. In order to match the higher accuracy of DFT method, a 6-31g basis set has been employed with the addition of (d,p) polarization functions (Wring & Hart, 1992). A simulation of the hydrazine detection has also been conducted on dimer and tetramer forms of ES to study the effect to the UV-VIS spectra generated through quantum mechanics calculations. The hydrazine detection occurs through a process called 'dedoping', where the nitrogen atom in ES chain loses its positive charge after going through electron delocalization. In this simulation, the dedoping process was demonstrated by carrying out a series of TD-DFT calculation on dimer and tetramer ES chains with a different assignments of positive charge, ranging from +1 to +4 and also +1 to +2 for tetramer and dimer of PANI chain respectively. As for multiplicity, the high spin multiplicity state was set to the ES chains based on ideas proposed by Stafström et al. in their seminary article that proposed the ES has a charged radical open-shell structure with a high spin state (Stafström et al., 1987)

4.1 Conformational Search

Conformational search were conducted to obtain an optimised structure of monomer, dimer, trimer and tetramer models of ES. Thus, the torsional angles of monomer, dimer, trimer and tetramer models of ES after a systematic torsion step of 30 degree is tabulated in Table 4.1.

Table 4.1: Dihedral scan with AM1 method

Ring	1 to 2	2 to 3	3 to 4	4 to 5	5 to 6	6 to 7	7 to 8
Monomer	-40.7421						
Dimer	-37.7655	46.2482	-42.4854				
Trimer	-37.1920	48.3166	-40.4427	49.8097	-48.4680		
Tetramer	-37.1110	48.6255	-35.6976	48.6713	-41.6178	41.8800	-47.1272

Based on the presented table, we can see that the minimum energy angles for neighbouring C_6H_4 rings show an alternation in sign along the backbone chain. The dihedral angles defined by the two adjacent rings averaging at 42^o. The alternation of the dihedral angles signs along the backbone chain is important to minimize the steric repulsion between neighbouring C_6 rings. The observed average minimum torsional angle is close to the value of torsional angle reported by Adrian Varela-Álvarez and co-workers who also have obtained alternate signs for adjacent rings along the chain, specifically 21.0^o, -39.0^o, 10.0^o and -37.2^o (Varela-Álvarez et al., 2005). MacDiarmid and co-worker reported that these angles strongly determine the relative intensities of the X-ray reflections. They discovered that the best torsional angle value that fits the experimental data is 30^o. Figure 4.1 shows the structures of the monomer, dimer, trimer and tetramer after a complete scan of the torsion angles. From the figure, it can be observed almost symmetrical arrangement of the structure of the repeating units.

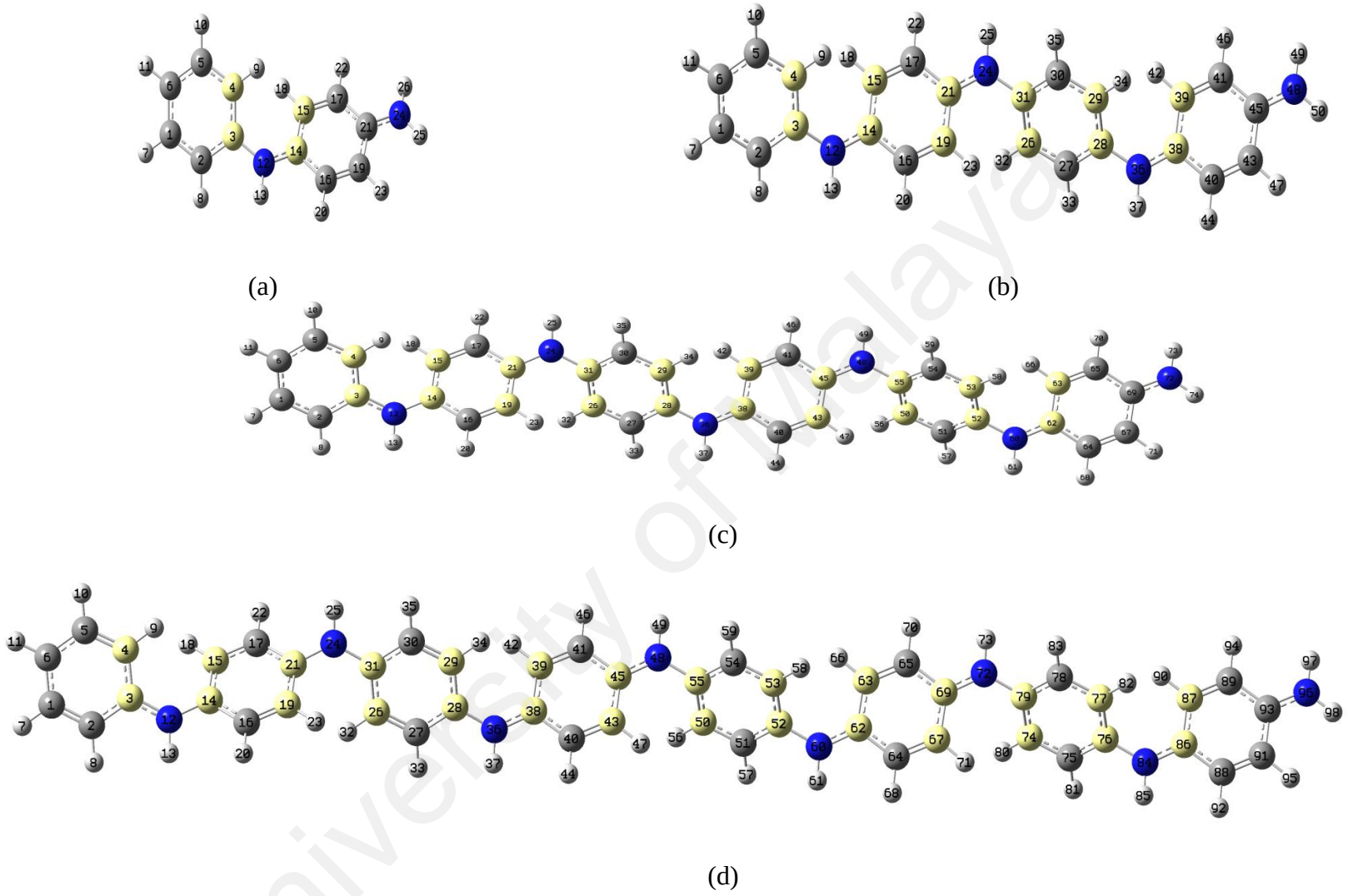

Figure 4.1: The structure of (a) monomer (b) dimer (c) trimer and (d) tetramer after systematic torsion step of 30 degree as highlighted on the carbon atoms used for the dihedral scan.

The energy of the monomer, dimer, trimer and tetramer after the complete dihedral scan are --0.335583 a.u., -0.753301 a.u., -1.199581 a.u., and -1.663149 a.u. respectively. The energies of the ES chains were observed to be decreased as the chain lengths are increased.

A further confirmation of the best structure has also been conducted by conducting potential energy scan (PES) using the dimer model with the same step size which is 30^{o}. The two different angles or scan coordinate (SC), SC1 and SC2, were varied and were calculated using AM1 method. The presented Figure 4.2 is the three dimension (3D) graph plotted by Gaussview 5 after a successful PES calculation. From the graph in the top view (Figure 4.2 (b)), four saddle points marked by the blue colour regions are observed. The four saddle points at about 1) SC1 = 100^{o}, SC2 = 125^{o} 2) SC1 = 100^{o}, SC2 = 275^{o} 3) SC1 = 275^{o}, SC2 = 100^{o} 4) SC1 = 275^{o}, SC2 = 275^{o}, composed of the same structures of dimer model have the lowest energy of -0.753301 a.u. which is the same energy as the manual torsion angle scan conducted.

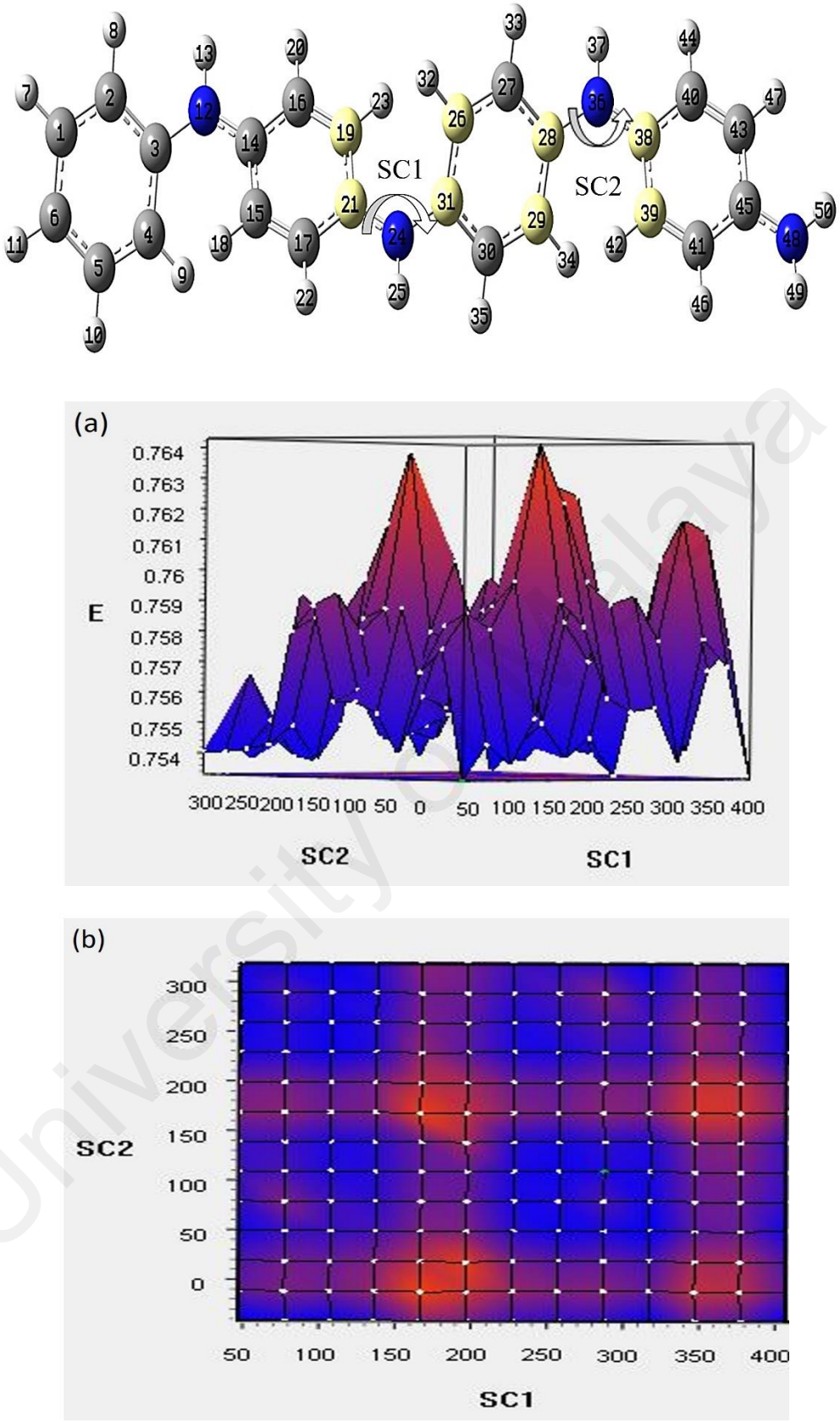

Figure 4.2: Gaussian scan grid with semi-empirical, AM1 method of a dimer from two different angles, SC1 and SC2 (a) side (b) top view.

The four geometries of the dimer ES are confirm to be of the exact same conformation based on superimposition. As shown in the Figure 4.3, after the superimposition of the four geometries, the image produced is exactly only one ES dimer model which indicates that all the geometries are aligned exactly on top of one another.

Figure 4.3: Superimposed image of four dimer configurations from the Gaussian scan.

Henceforth, the lowest energy structure from the torsional scan for all the different degres of polymerizarion is then further optimized using a better computational method - DFT with the B3LYP functional.

4.2 Optimization

DFT method with B3LYP functional together with the 6-31G (d,p) basis set has been employed to perform optimisation calculation on monomer, dimer, trimer and tetramer ES models.

Table 4.2: Optimized energy for different degree of polymerisation of ES.

ES	Monomer	Dimer	Trimer	Tetramer
Optimized energy (a.u.)	-573.807094	-1146.351390	-1718.868898	-2291.368829

As expected, upon further optimisation of the monomer, dimer, trimer and tetramer the energies follow the trend of the energy produced from the complete torsion angle scan but with a significant difference in the computed optimised energy. The optimised energies of the ES models are decreased as the degree of the polymerisation is increased from -573.807094 a.u.. for monomer ES to -2291.368829 a.u. for tetramer ES, whilst the optimised energy for dimer ES and trimer ES are -1146.351390 a.u. and -1718.868898 a.u., respectively. The decreasing of the optimised energy as the backbone chain length is increased suggests that the ES model becomes more stable as the degree of polymerisation for ES model is increased. The pattern of the stability increment with the increase in the degree of polymerisation is similar with the work published by Carlos Alemán and co-worker who also observed stability increase with increase in the chain length from n=5 to n=13 (Alemán et al., 2008).

4.3 Time dependent-self consistent field calculation

4.3.1 Effect of different degrees of polymerisation

The energy difference between the HOMO and LUMO, the HOMO-LUMO gap, in a molecular system is related to the wavelengths of the light that a polymer can absorb and this was investigated next. As shown in Figure 4.4 for both HOMO and LUMO configuration, the electron density is distributed all along the optimised structure of monomer, dimer, trimer as well as tetramer of ES PANI.

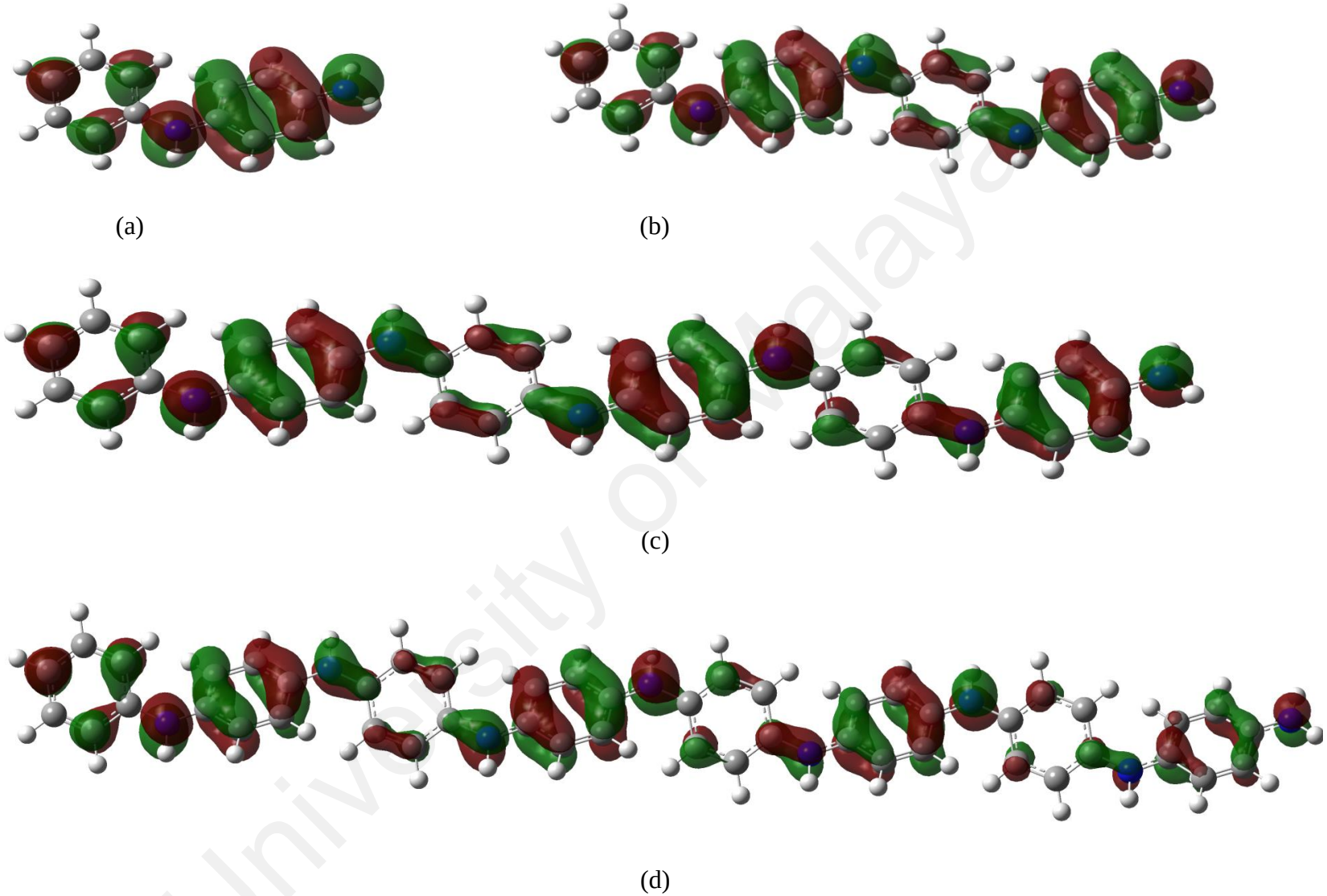

(a) (b)

(c)

(d)

Figure 4.4: HOMO and LUMO structure of (a) monomer, (b) dimer, (c) trimer and (d) tetramer model of ES PANI.

The conjugated system of ES, accompanied by the appropriate dihedral angles has made the electron able to be delocalised throughout the chain, thus increasing its ability to become a conducting polymer. Referring to the Figure 4.5, the energy difference between HOMO and LUMO or band gap for the optimised tetramer (n = 4) ES is lower than optimised dimer ES (n = 1). Notice that the band gap for monomer ES is 4.71eV while the band gap for tetramer ES is 3.88 eV.

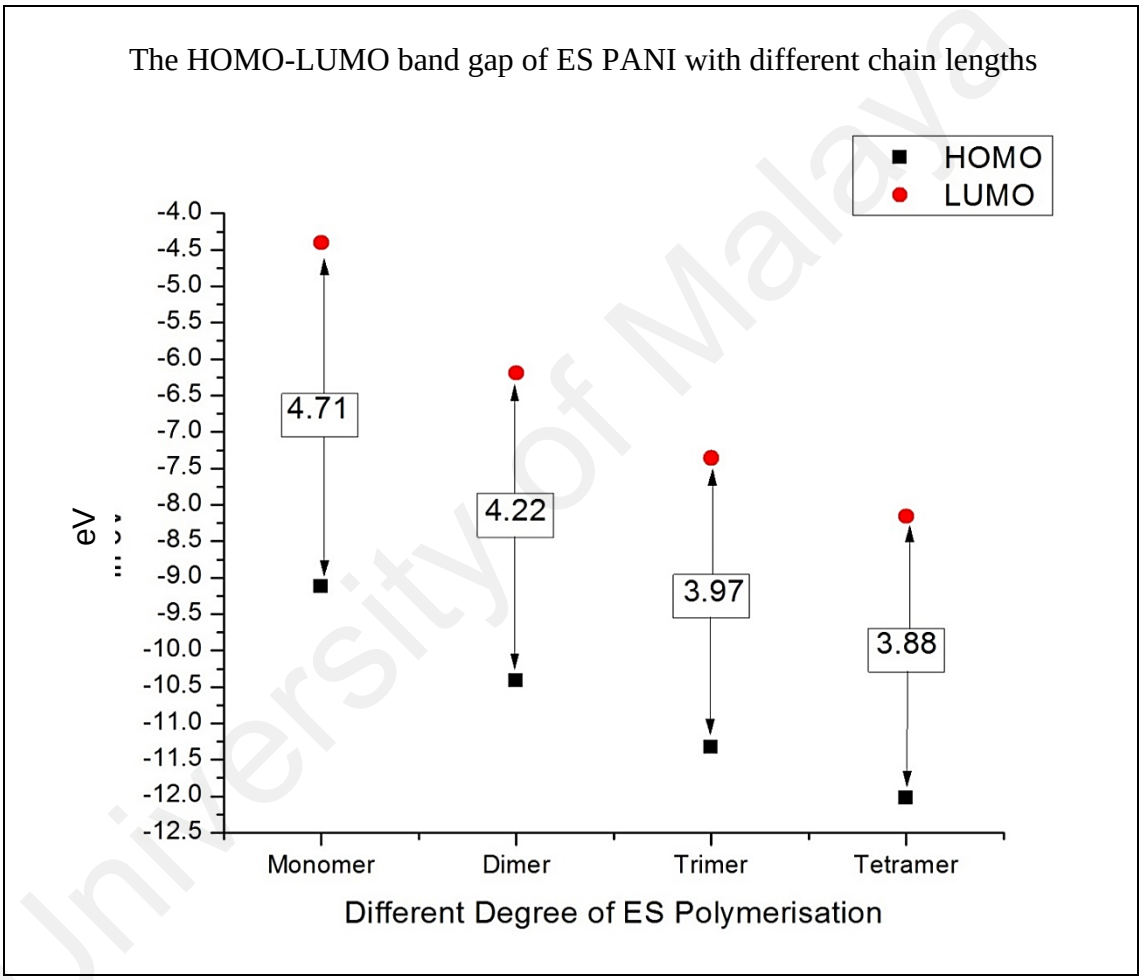

Figure 4.5: The HOMO-LUMO band gap of ES PANI with different chain lengths.

The pattern of the band gaps that are being recorded is in agreement with the previous work carried out by Carlos Alemán and co-workers who stated that the ES PANI band gap decreased from 2.52 to 1.53 eV when the number of ES PANI ring increases from 5

to 11 (Alemán et al., 2008). Likewise, the experimental band gap value observed by W.S Huang and A.G MacDiarmid is 1.5 eV due to the transition from the Π-polaron band (Huang & Diarmid, 1992). Decrease in band gap value makes the polymer to become a much better conductor due to the easiness for the electron to move between HOMO and LUMO levels.

In order to compare the calculated results with experiments, Figure 4.6 illustrates a UV spectrum (Kavirajaa et al., 2014) with a significant peak around 784 nm.

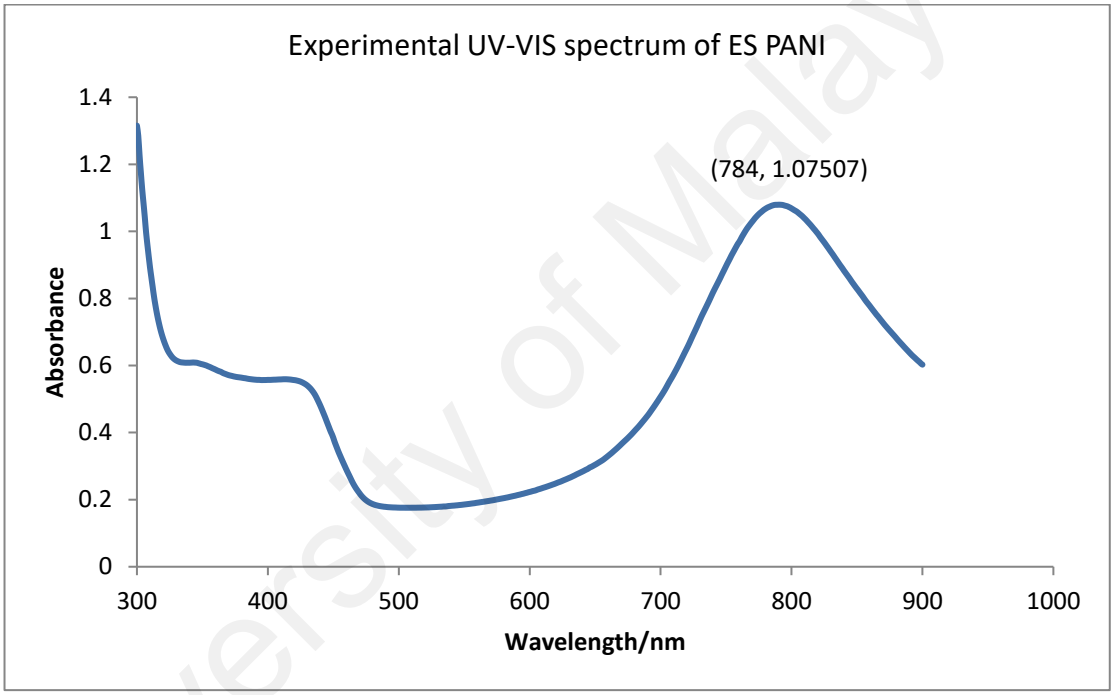

Figure 4.6: Experimental UV-VIS spectrum of ES PANI (Kavirajaa et al., 2014).

This is the peak of the ES PANI that has been doped with the counter ion AOT^- and ES PANI is in a thin film form. The intense peak is due to the existence of the polaron from the attraction of the positively charge nitrogen atom and negatively charge oxygen atom of the AOT^-. After hydrazine was introduced to the complex, a sudden reduction of the peak intensity was observed (data not included). This is because the polaron is absent as ES is now transformed into EB, which means that the nitrogen in the ES PANI chain

is no longer positively charge and it is no longer attracted to the AOT^-. The presence of hydrazine which is more positively charged than the nitrogen in the ES PANI chain has taken the AOT^- from the ES PANI chain thus causing electron delocalization in the ES PANI chain leaving the nitrogen atom in the ES PANI chain to be neutral. Figure 4.7 explains the dedoping process, and included in the figure are the simulated structures of ES PANI with different charges. The charges was distributed throughout the molecules and the Mulliken charges at each atom were tabulated in Appendix B.

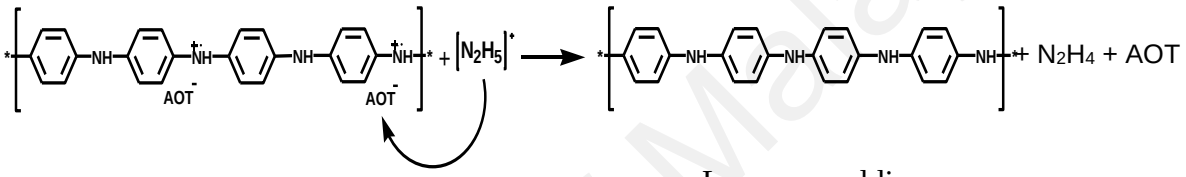

Emeraldine salt

Leucoemeraldine

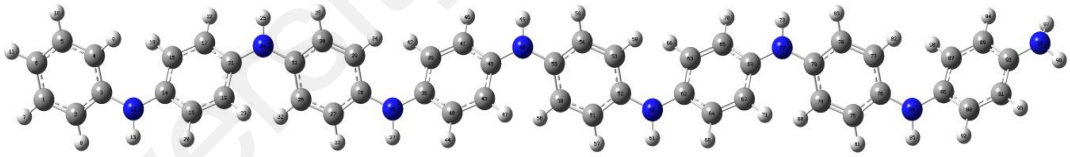

(a) +1 charges

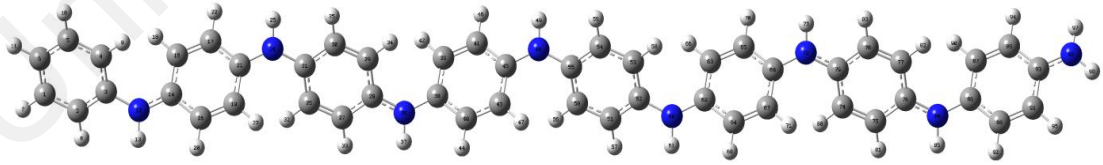

(b) +2 charges

Figure 4.7: Dedoping process of ES PANI with AOT^- and simulated structures of (a) +1 charges, (b) +2 charges, (c) +3 charges, and (d) +4 charges respectively.

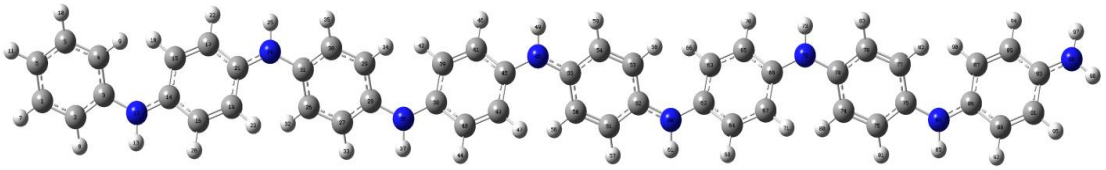

(c) +3 charges

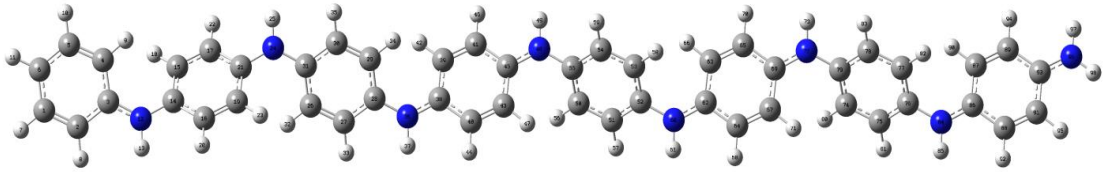

(d) +4 charges

Figure 4.7, continued

Table 4.3: Dihedral angle of tetramer ES with different charge assigned.

`	Charge	1 to 2	2 to 3	3 to 4	4 to 5	5 to 6	6 to 7	7 to 8
Tetramer	1	-42.9003	42.1424	-41.6340	40.8470	-41.3385	40.8094	-44.7737
	2	-42.8182	37.7825	-40.5714	42.1550	-42.1740	39.5559	-38.7829
	3	-39.7687	40.3375	-40.4560	37.3357	-39.6930	40.0858	-38.1430
	4	-37.1110	48.6235	-35.6977	48.6707	-41.6177	41.8801	-47.1272

Referring to Figure 4.7, the different charge assigned to the ES PANI didn't significantly affect the ES PANI conformation. However, taking a closer look to the values of the dihedral angle, as presented in Table 4.3, we can see that they are actually slightly different. This is due the fact that the different number of positive charge assigned to the ES PANI make the formal charge of the ES PANI changed, thus, resulting in the changes of bond order and eventually bonds length, which finally caused the slightly changes of the ES PANI structure as well as the dihedral angle (Glendening & Weinhold, 1997).

UV-VIS spectrum of ES was investigated with different degrees of polymerization from n = 1-4 where benzoid and quinoid ratio in the chain was about 1:1. From Figure 4.8 and Table 4.4, it is acknowledged that the increase in the number of ring of the ES

caused the UV-VIS spectrum to experience a red shift. The wavelength for the most significant peak of monomer is 318.0 nm while the wavelength for the most intense peak of tetramer is 1072.0 nm. Within the entire wavelength, dimer ES shows the closest value of excitation energy to the experimental data which is around 800 nm. Notice that the calculated dimer wavelength is in a good agreement with the work published by Zhekova and co-workers who have found the highest intensity spectral lines of shorter wavelength about 800 nm for green colour ES (Zhekova et al., 2007).

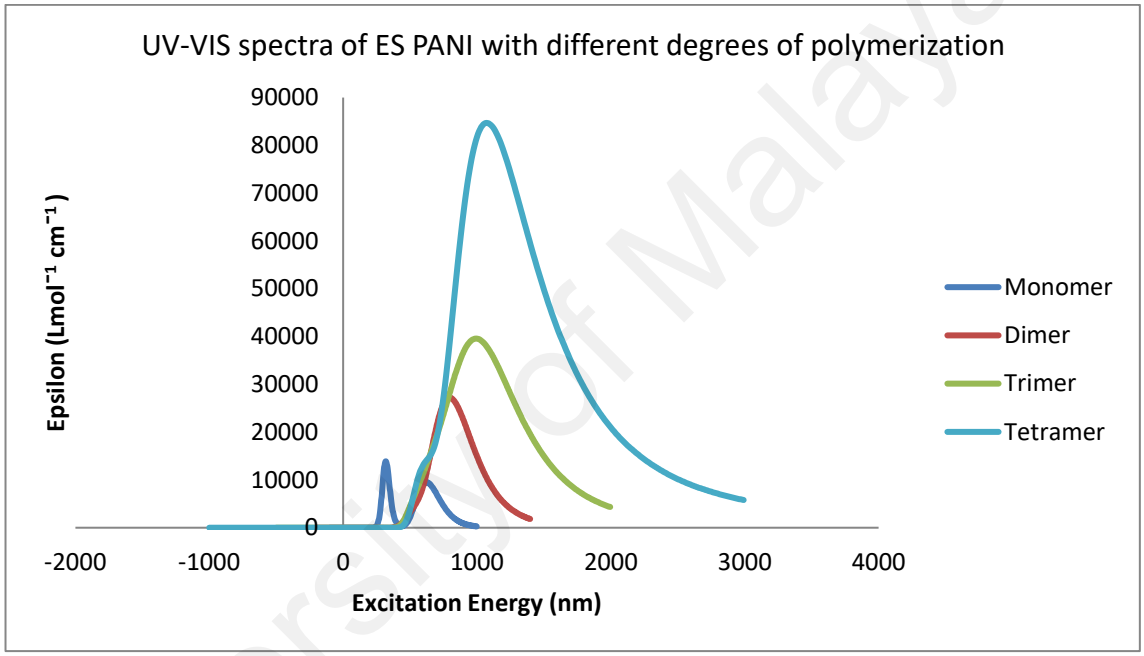

Figure 4.8: UV-VIS spectra of ES PANI with different degrees of polymerization.

Table 4.4: Epsilon maximum (λ_{max}) of ES PANI with different degrees of polymerization.

	Monomer	Dimer	Trimer	Tetramer
λ_{max} (nm)	318.0	795.2	995.0	1072.0

4.3.2 Different calculation methods

Further work has been conducted to find the most compatible method which gives the closest results of ES UV-VIS peak to experimental investigation. Thus, several different computational methods such as semi-empirical methods, namely AM1 and PM6, and also higher accuracy methodologies such as Time Dependant-Density Functional Theory (TD-DFT) namely B3LYP, CAM-B3LYP, LSDA, M062X and PBEPBE have been employed in the TD-SCF calculation of the dimer ES. Notice that the TD-DFT method in Gaussian09 includes a new functional called the exchange-correlation kernel which is more convenient considering that it is a fuctional of the ground-state density alone. The output of the TD-SCF calculation has been studied for the UV-VIS spectra simulated on top of the difference in the band gap produced via the different calculation methods. As presented in the Figure 4.9 and Table 4.5, semi-empirical AM1, PM6 and also DFT B3LYP show the most reliable UV-VIS absorption peak simulation which are 796.0 nm, 785.0 nm and 795.2 nm and this is comparable with the experimental data which recorded a significance peak around 784.0 nm (Kavirajaa et al., 2014).

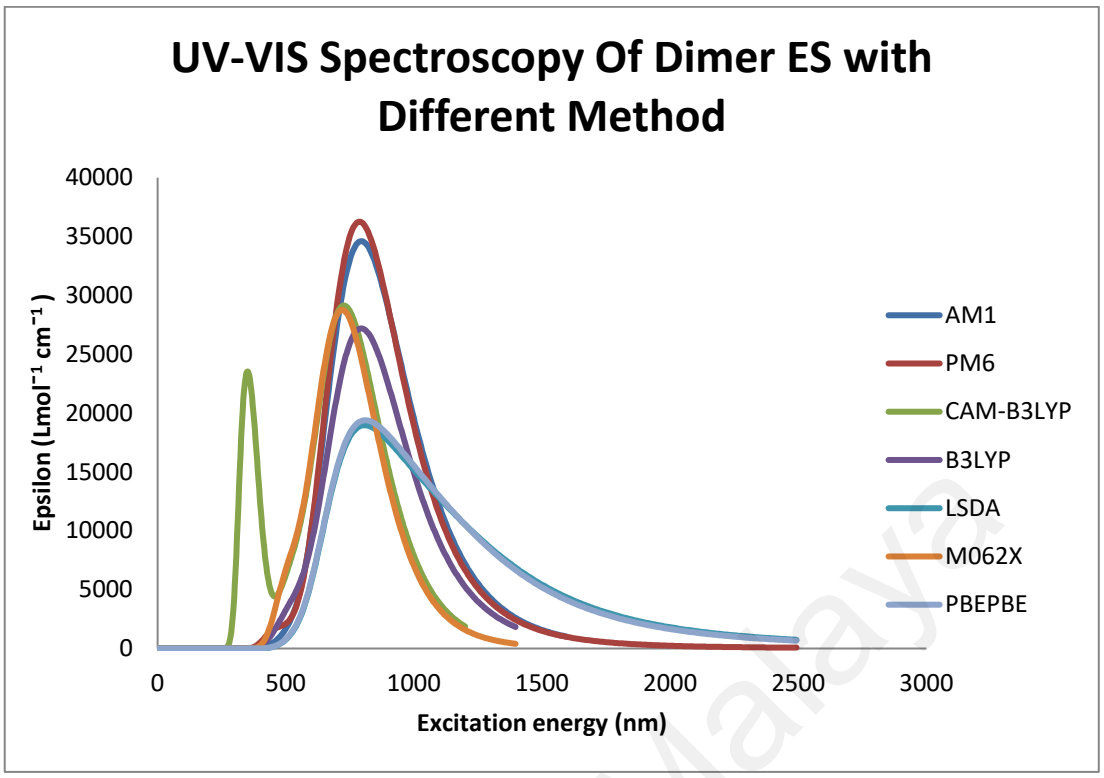

Figure 4.9: UV-VIS spectra of dimer ES with different calculation methods.

Table 4.5: Epsilon maximum (λ_{max}) of ES PANI with different calculation methods.

	Exp. (Kavirajaa et al., 2014)	AM1	PM6	CAM-B3LYP	B3LYP	LSDA	MO62X	PBEPBE
λ_{max} (nm)	784.0	796.0	785.0	726.8	795.2	806.0	718.4	813.0

On the other hand, the band gaps plotted in Figure 4.10 indicate that the AM1 method has the largest band gap value which is 7.57 eV while the LSDA method posses the lowest band gap value, which is 4.92 eV lower than the AM1 band gap value. The significantly different band gaps value observed from AM1 and LSDA method used is due to the fact that the algorithm used in this methodology the method does not encompass additional electron correlation effects,whilst in excitation spectra calculation, diffuse functions are very vital.

Notice that B3LYP which produced a relatively reliable UV-VIS significant peak of ES has a band gap value of 4.22 eV. Likewise, the band gap value for B3LYP calculation

found is almost similar to the value observed by Varela-Álvarez A. and Sordo J. A. who predicts a Π-Π* band gap of 4.30 eV but with a different method of calculation, namely PBEh/6-31G(d,p), which they reported had agreed reasonably well with x-ray information and optical absorption data for ES which recorded a Π-Π* band gap of 3.80 eV (Varela-Álvarez & Sordo , 2008).

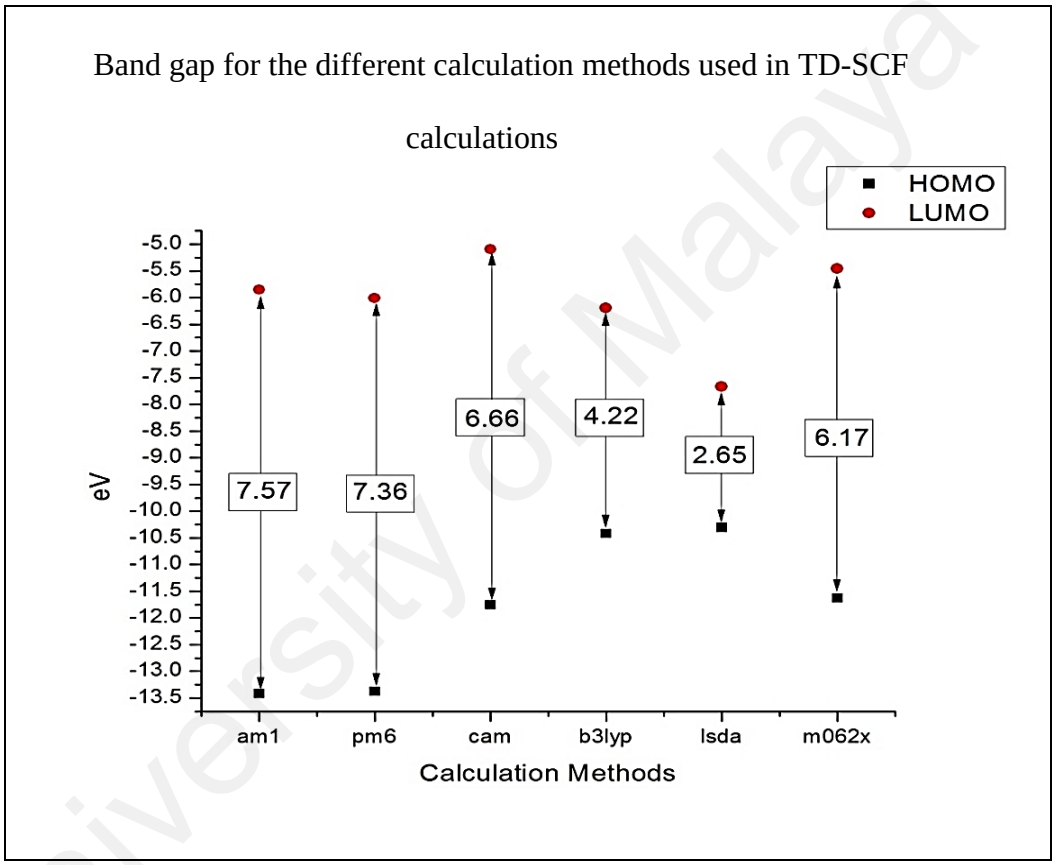

Figure 4.10: Band gap for the different calculation methods used in TD-SCF calculations.

4.3.3 Hydrazine detection simulation

The method that provided the UV peak for ES which is close to the experimental value was then selected for further simulation of the hydrazine detection. In other words, the simulation of the dedoping process or positive charged reduction process. This is because, in the presence of hydrazine, the AOT^- is extracted from the ES chain which eventually causes electron delocalisation. Consequently, the positive charge on the chain backbone will be reduced. The dedoping or charge reduction process was simulated using TD-SCF calculation with AM1, PM6 and B3LYP computational methodologies.

Roughly, from Figures 4.11 to 4.13 presented, we could see that as the positive charge in the backbone chain of ES is reduced, the intensities of the significant peaks are also reduced besides having a red shift. However, a closer look into the details of the λ_{max} as well as the peak intensities, it revealed that in the AM1 and PM6 calculation methods, the significant peak for tetramer ES undergoes a blue shift when the postive charge is reduced from +3 to +2. As tabulated in the Table 4.6, the λ_{max} for +3 charge of AM1 and PM6 methods are 1310.0 nm and 1250.0 nm respectively. Meanwhile, the λ_{max} value of the +2 charge for AM1 is 1248.0 nm and for PM6, the value is 1232.0 nm. On the other hand, the significant peak intensities of tetramer ES for PM6 calculations are also slightly off the experimental data observed. This is because the λ_{max} value of the significant peak of the +2 charge is slightly higher than the value of +3 charge significant peak which are 71174.5 nm and 70524.6 nm respectively.

Henceforth, it can be concluded that the AM1 and PM6 method calculations for tetramer ES provide output of calculations that are not comparable with the experimentally observed data. The phenomena of reduced absorbance and red shift in the UV-VIS spectrum can be explained by considering what happened in the dedoping. The absorbance value decreased because the doping level in the backbone chain is reduced due to the presence of the hydrazine. The red shift observed is an indication of the increase

in conjugation within the system (Kavirajaa et al., 2015). Theoretically, increased conjugation brings the HOMO and LUMO orbitals closed together, thus, less energy (ΔE) is needed to cause the electron promotion and eventually make the wavelength that provides this energy to be increased. These could be explained through the equation $\lambda = \frac{hc}{\Delta E}$.

Conversely, the dedoping process simulation of tetramer ES using the B3LYP methodology is in good agreement with the experimental data. The UV-VIS spectrum simulated shows a bathochromic shift as well as the reduction of the peak intensities as the positive charge in the backbone chain is reduced.

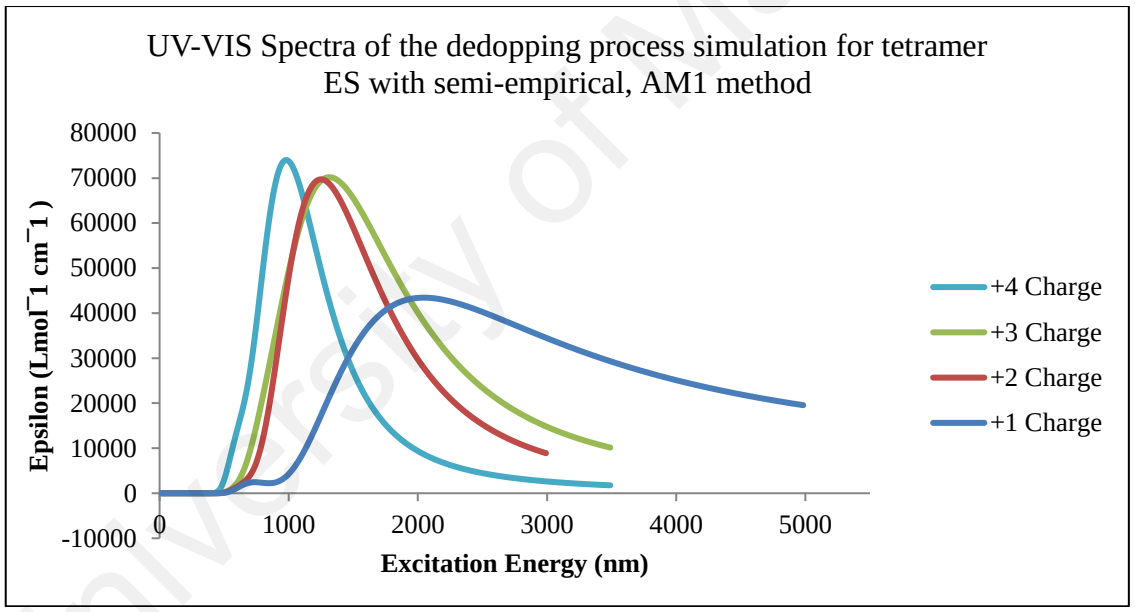

Figure 4.11: UV-VIS spectra of the dedoping process simulation for tetramer ES with semi-empirical, AM1 method.

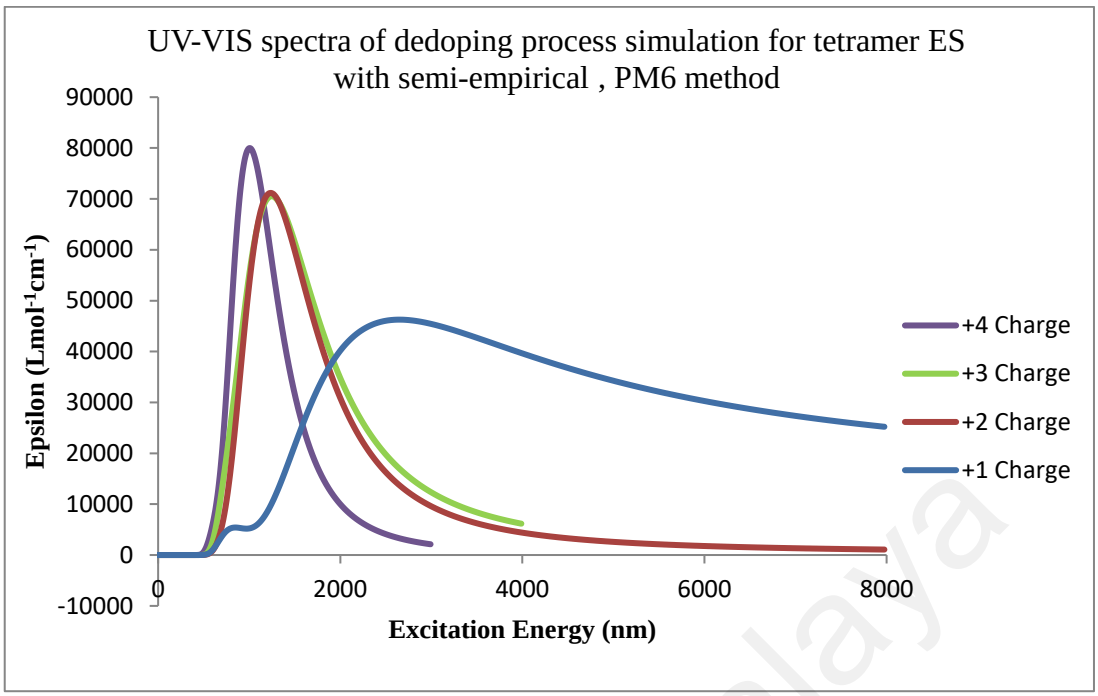

Figure 4.12: UV-VIS spectra of dedoping process simulation for tetramer ES with semi-empirical, PM6 method.

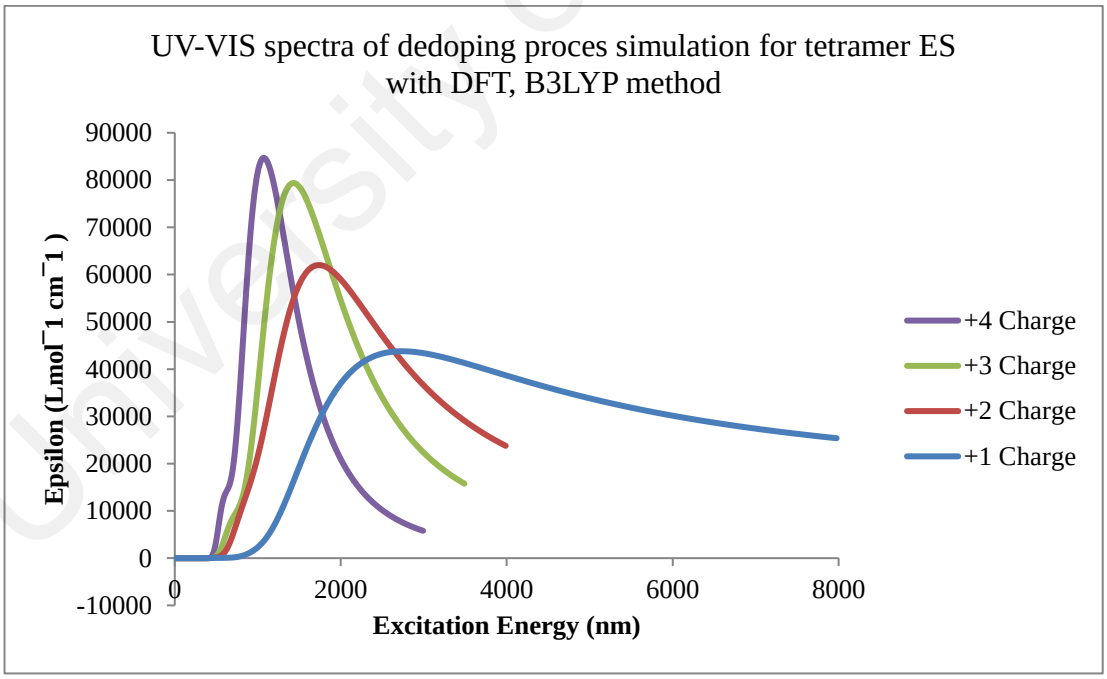

Figure 4.13: UV-VIS spectra of dedoping process simulation for tetramer ES with DFT, B3LYP method.

Table 4.6: The λ_{max} and epsilon ($Lmol^{-1}$ cm^{-1}) of tetramer and dimer ES with different assigned charges.

Charge		λmax (nm)			epsilon ((Lmol^{-1} cm^{-1})		
		AM1	PM6	B3LYP	AM1	PM6	B3LYP
Tetramer	4+	980.0	1008.0	1072.0	73990.55	79990.01	84697.46
	3+	1310.0	1250.0	1430.0	70183.73	70524.62	79367.12
	2+	1248.0	1232.0	1732.0	69712.50	71174.52	62011.28
	1+	2040.0	2648.0	2744.0	43431.79	46269.43	43780.35
Dimer	2+	796.0	785.0	795.2	34604.28	36260.91	27192.87
	1+	1906.0	1058.0	1650.0	30393.51	23072.66	20302.17

The UV-VIS spectra of the dedoping process simulation conducted on dimer ES with the same three methodologies - AM1, PM6 and B3LYP - show the same pattern but with a different value of the significant peak and λ_{max}. As displayed in Figures 4.14 to 4.16, the trend of the spectra is similar with the experimentally observed UV-VIS spectrum obtained by Kavirajaa et al. Based on the UV-VIS spectra plotted from the dedoping process simulation, its seems that as the backbone chain positive charge is reduced from +2 charge to +1 charge, the intensities of the significant peaks are reduced and the spectra plotted are also experiencing bathochromic shifts.

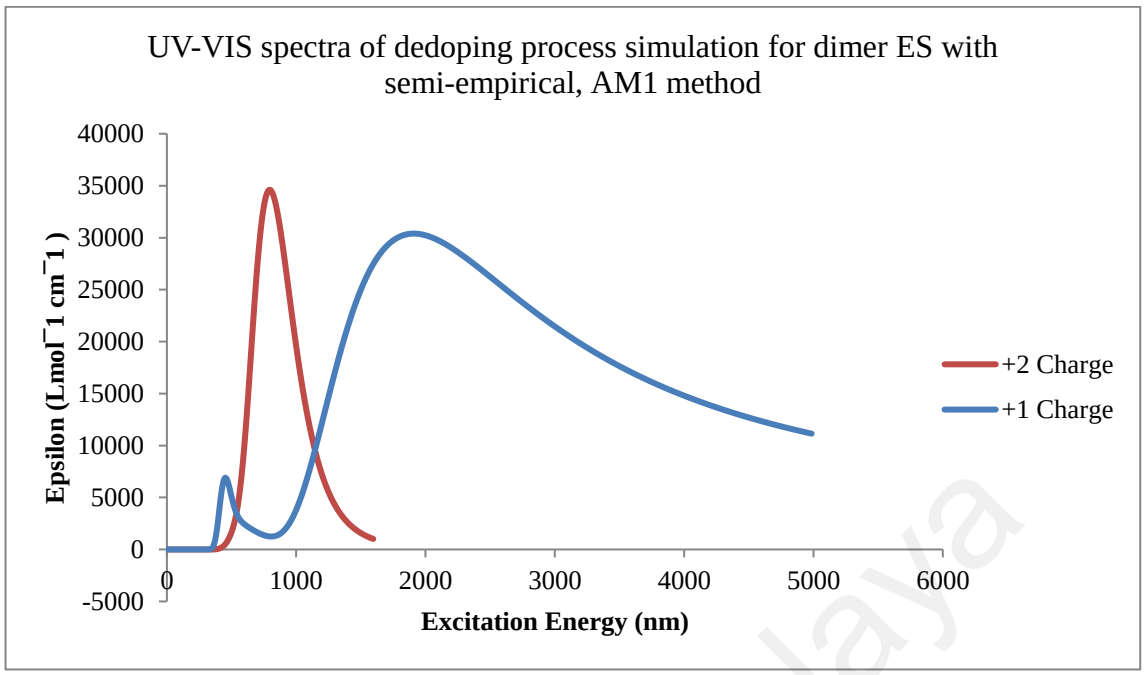

Figure 4.14: UV-VIS spectra of dedoping process simulation for dimer ES with semi-empirical, AM1 method.

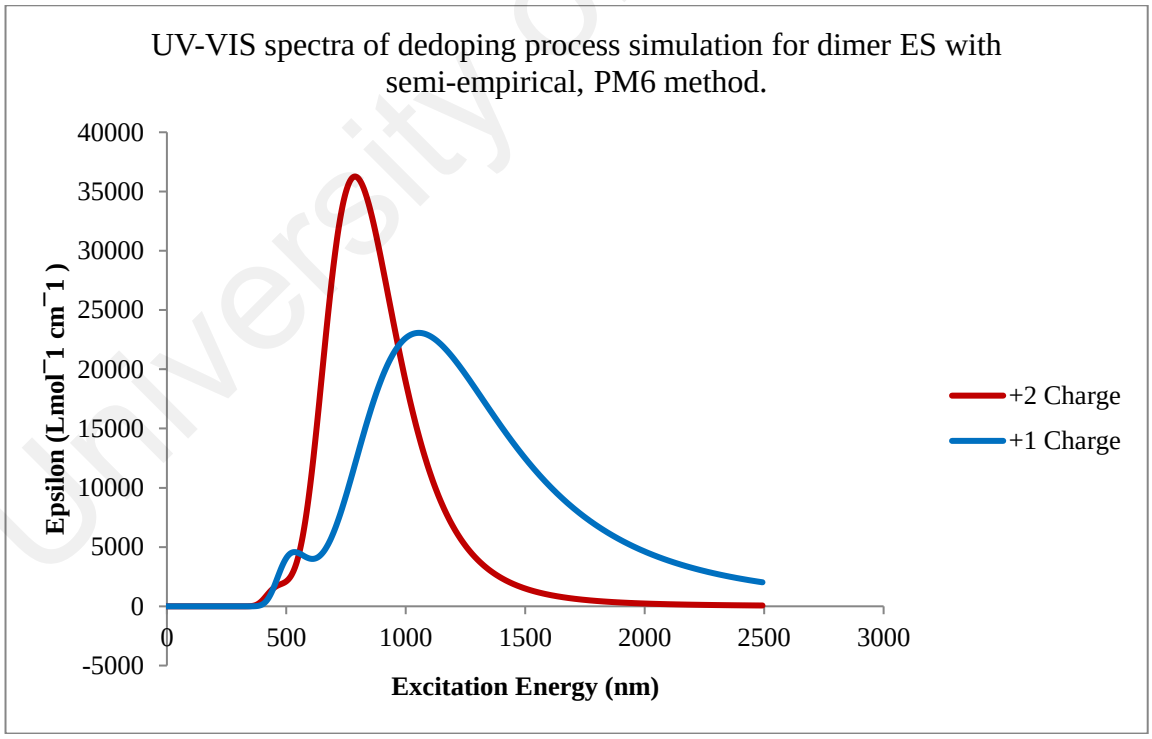

Figure 4.15: UV-VIS spectra of dedoping process simulation for dimer ES with semi-empirical, PM6 method.

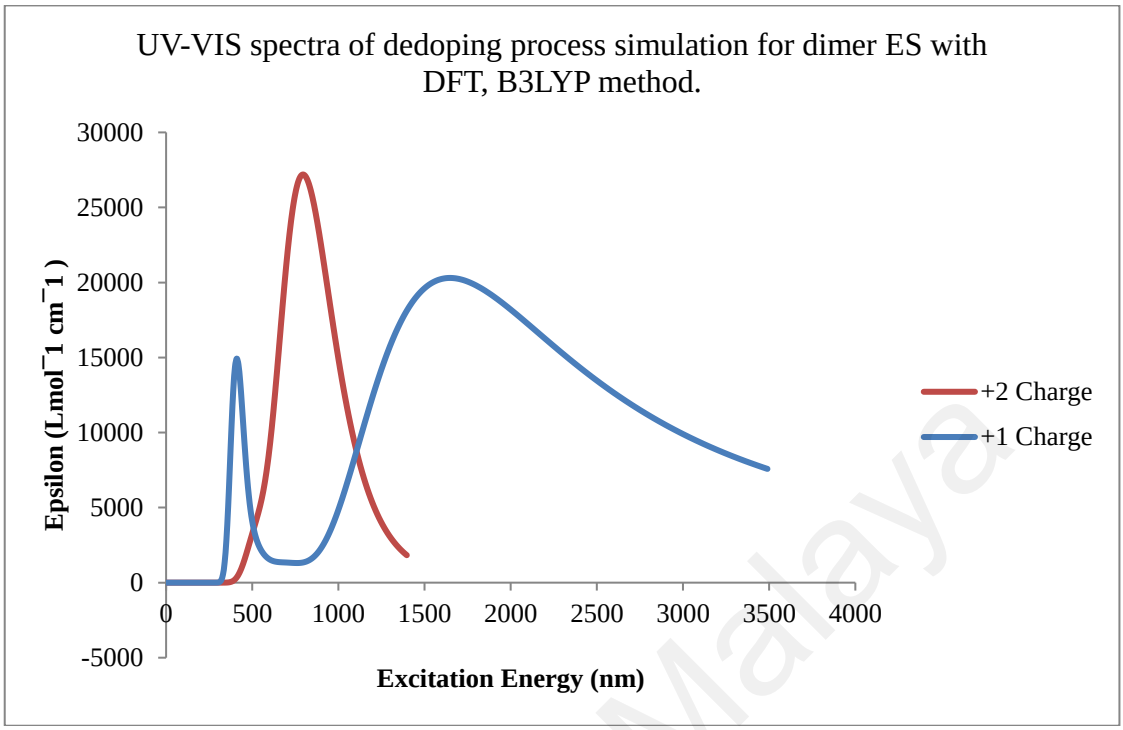

Figure 4.16: UV-VIS spectra of dedoping process simulation for dimer ES with DFT, B3LYP method.

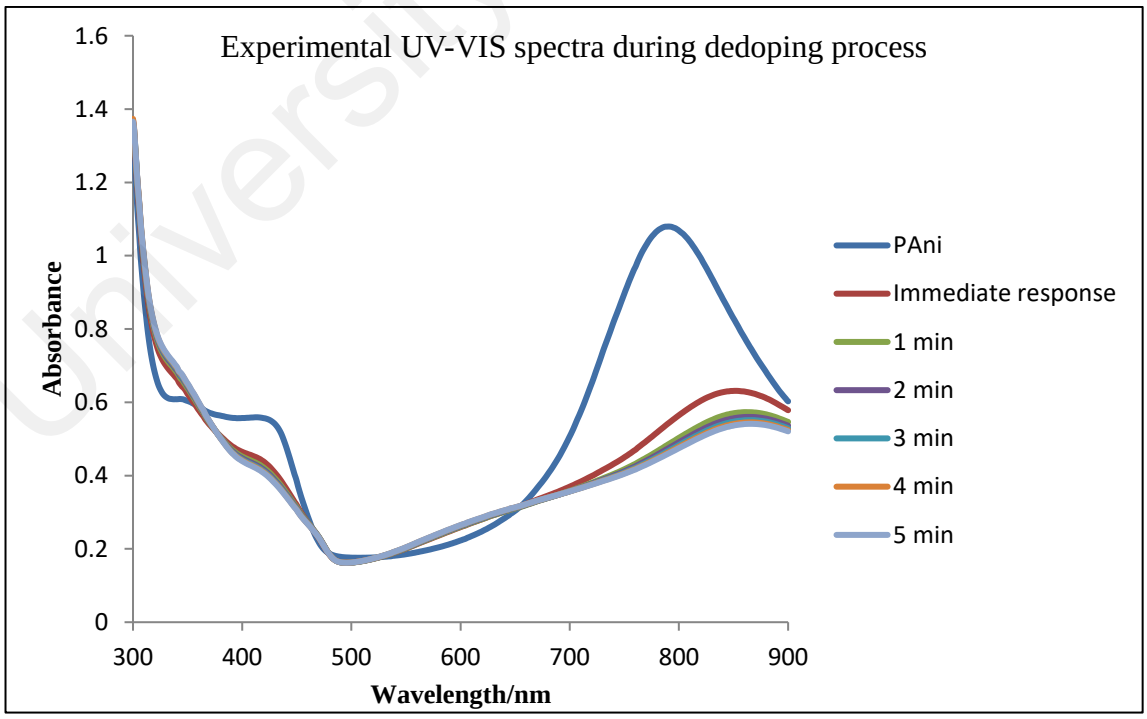

Figure 4.17: Experimental UV-VIS spectra during dedoping process (Kavirajaa et al., 2014).

CHAPTER 5: CONCLUSION

Ab initio calculations with DFT (B3LYP, CAM-B3LYP, LSDA and MO62X) and semi-empirical (AM1 and PM6) methods have been explored for UV-VIS spectral calculations for emeraldine salt of polyaniline. Based on the conformational search results, the connected rings are observed to exhibit an average torsional angle of 43.26 degrees, alternating in sign along the backbone chain. This alternation is responsible for the minimum steric repulsion between neighbouring C_6 rings. Besides, increasing the degree of polymerisation makes the wavelength of the main peak of the spectra to experience red shifts. Among all different degrees of polymerisation of the calculated ES, dimer ES which composed of 4 rings with a ratio of 1:1 benzoid and quinoid shows ES UV-VIS closest to experimentally observed results. On the other hand, semi-empirical AM1, PM6 and also DFT B3LYP show the most reliable UV-VIS absorption peak simulation using the dimer model in comparison with the experimental data recorded by Kavirajaa and co-worker. Meanwhile, the dedoping process simulation conducted on tetramer and dimer ES, shows that B3LYP functional with a basis set 6-31g(d,p) gives the most promising results for the tetramer ES simulation. Nevertheless, in general, the results for the calculations of the dedoping process using AM1, PM6 and DFT B3LYP are found to exhibit similar patterns and are in good agreement with experimental data.

REFERENCES

Alemán, C., Ferreira, C. A., Torras, J., Meneguzzi, A., Canales, M., Rodrigues, M. A., & Casanovas, J. (2008). On the molecular properties of polyaniline: A comprehensive theoretical study. *Polymer*, *49*(23), 5169-5176.

Atassi, Y., Tally, M., & Ismail, M. (2008). Synthesis and characterization of chloride doped polyaniline by bulk oxidative chemical polymerization. Doping effect on electrical conductivity. *arXiv preprint arXiv:0809.3552*.

Audrieth, L. F., & Ogg, B. A. (1951). *The chemistry of hydrazine*. New York: Wiley.

Banwell, C. N., & McCash, E. M. (2008). *Fundamentals of molecular spectra*. London, UK: McGraw-Hill.

Bovey, F. A., & Winslow, F. H. (Eds.). (1979). *Macromolecules: An Introduction to Polymer Science*. New York, NY: Academic Press Inc.

Bower, D. I., (2002). *An Introduction to Polymer Physics*. New York: Cambridge University Press.

Bredas, J. L., & Street, G. B. (1985). Polarons, bipolarons, and solitons in conducting polymers. *Accounts of Chemical Research*, *18*(10), 309-315.

Chiang, J. C., & MacDiarmid, A. G. (1986) Polyaniline: protonic acid doping of the Emeraldine form to the metallic regime. *Synthetic Metals*, *13*(1), 193-205.

Choudhary, G., & Hansen, H. (1998). Human health perspective of environmental exposure to hydrazines: A review. *Chemosphere*, *37*(5), 801-843.

Dewar, M. J., Zoebisch, E. G., Healy, E. F., & Stewart, J. J. (1985). Development and use of quantum mechanical molecular models. 76. AM1: a new general purpose quantum mechanical molecular model. *Journal of the American Chemical Society*, *107*(13), 3902-3909.

Diaz A.F., Kanazawa K.K., & Gardini G.P. (1979). Electrochemical polymerization of pyrrole. *Journal of the Chemical Society, 14*, 635- 636.

EngineersGarage. Sensors: Different Types of Sensors. (2012). Retrieved on June 16, 2016 from http://www.engineersgarage.com/articles/sensors.

Fleming, I. (2009). *Molecular orbitals and organic chemical reactions Student Edition*. Wiley.

Frängsmyr, T., & Malmström, B. G. (1992). *Nobel lectures in chemistry, 1981-1990*. Farrer Road, Singapore: World Scientific.

Freund, M. S., & Deore, B. A. (2007). *Self-doped conducting polymers*. London, UK: John Wiley & Sons.

Frisch, M. J., Trucks, G. W., Schlegel, H. B., Scuseria, G. E., Robb, M. A., Cheeseman, J. R., Scalmani, G., Barone, V., Mennucci, B., Petersson, G. A., Nakatsuji, H., Caricato, M., Li, X., Hratchian, H. P., Izmaylov, A. F., Bloino, J., Zheng, G., Sonnenberg, J. L., Hada, M., Ehara, M., Toyota, K., Fukuda, R., Hasegawa, J., Ishida, M., Nakajima, T., Honda, Y., Kitao, O., Nakai, H., Vreven, T., Montgomery, J. A. Jr., Peralta, J. E., Ogliaro, F., Bearpark, M., Heyd, J. J., Brothers, E., Kudin, K. N., Staroverov, V. N., Kobayashi, R., Normand, J., Raghavachari, K., Rendell, A., Burant, J. C., Iyengar, S. S., Tomasi, J., Cossi, M., Rega, N., Millam, J. M., Klene, M., Knox, J. E., Cross, J. B., Bakken, V., Adamo, C., Jaramillo, J., Gomperts, R., Stratmann, R. E., Yazyev, O., Austin, A. J., Cammi, R., Pomelli, C., Ochterski, J. W., Martin, R. L., Morokuma, K., Zakrzewski, V. G., Voth, G. A., Salvador, P., Dannenberg, J. J., Dapprich, S., Daniels, A. D., Farkas, Ö., Foresman, J. B., Ortiz, J. V., Cioslowski, J. & Fox, D. J. (2009). Gaussian 09, Wallingford, USA.

Frisch, A. E., & Foresman, J. B. (1996). *Exploring Chemistry with Electronic Structure Methods*. Pittsburgh PA: Gaussian Inc, 302.

Fried, J. R., (2014). *Polymer Science and Technology, 3rd Edition*. New Jersey, USA: Prentice Hall.

Glendening E. D., Weinhold, F. Natural Resonance Theory: II. Natural Bond Order and Valency. *Journal of Computational Chemistry*. *19*(6), 610-627.

Grinter, H. C., & Threlfall, T. L. (1992). *UV-VIS Spectra and Its Applications.* Berlin: Springer-Verlag.

Harrison, N. M. (2003). An introduction to density functional theory. *Nato Science Series Sub Series III Computer and Systems Sciences*, 187, 45-70.

H. J. Letheby (1862) On the production of a blue substance by the electrolysis of sulphate of aniline. *Journal of the Chemical Society, 15*, 161–163.

Huang, W. S., & MacDiarmid, A. G. (1993). Optical properties of polyaniline. *Polymer*, *34*(9), 1833-1845.

Kahn K., (2006). Semiempirical Quantum Chemistry. Retrieved from http://people.chem.ucsb.edu/kahn/kalju/chem226/public/semiemp_intro.html

Kavirajaa, P. S., Sharifah M., & Phang S.W. (2014) Enhancement of polyaniline properties bydifferent polymerization temperatures in hydrazine detection. *Journal of Applied Polymer Science*. *132*(13).

Kavirajaa, P. S., Sharifah M., & Phang S.W. (2015) Effect of dopant concentration on polyaniline for hydrazine detection. *Journal of Material Science in Semiconductor Processing*. *33*,24-31.

Ltd., K. S. (2016). Chemicals : World of Chemicals. Retrieved from World of Chemicals: http://www.worldofchemicals.com/chemicals/chemical-properties/hydrazine.html

Lewars, E. G., (2011*). Computational Chemistry: Introduction to the Theory and Applications of Molecular and Quantum Mechanics, 2nd Edition*. Dordrecht Heidelberg London New York: Springer.

Molapo, K. M., Ndangili, P. M., Ajayi, R. F., Mbambisa, G., Mailu, S. M., Njomo, N., ... Iwuoha, E. I. (2012). Electronics of conjugated polymers (I): polyaniline. *International Journal of Electrochemical Science*, *7*(12), 11859-11875.

Nasirian, S., & Milani Moghaddam, H. (2014). Effect of different titania phases on the hydrogen gas sensing features of polyaniline/TiO2 nanocomposite. *Polymer (United Kingdom)*, *55*(7), 1866–1874.

Nasirian, S., & Milani Moghaddam, H. (2014). Hydrogen gas sensing based on polyaniline/anatase titania nanocomposite. *International Journal of Hydrogen Energy*, *39*(1), 630–642.

Nascimento, G. M., Kobata, P. Y., Millen, R. P., & Temperini, M. L. (2007). Raman dispersion in polyaniline base forms. *Synthetic Metals*, *157*(6), 247-251.

Ravichandran, K., & Baldwin, R. P. (1983). Liquid chromatographic determination of hydrazines with electrochemically pretreated glassy carbon electrodes. *Analytical Chemistry*, *55*(11), 1782-1786.

Romanova, J., Madjarova, G., Tadjer, A., & Gospodinova, N. (2011). Solvent polarity and dopant effect on the electronic structure of the emeraldine salt. *International Journal of Quantum Chemistry*, *111*(2), 435-443.

Sambasevam, K. P., Mohamad, S., & Phang, S. W. (2015). Enhancement of polyaniline properties by different polymerization temperatures in hydrazine detection. *Journal of Applied Polymer Science*, *132*(13), 1–8.

Shieh, J., Huber, J. E., Fleck, N. A., & Ashby, M. F. (2001). The selection of sensors. *Progress in Materials Science*, *46*(3), 461-504.

Sholl, D., & Steckel, J. A. (2011). *Density functional theory: a practical introduction*. John Wiley & Sons.

Stafström, S., Brédas, J. L., Epstein, A. J., Woo, H. S., Tanner, D. B., Huang, W. S., & MacDiarmid A. G. (1987). Polaron Lattice in Highly Conducting Polyaniline: Theoretical and Optical Studies. *Physical Review Letters. 59*(13), 1464-1467.

Stewart, J. J. (2007). Optimization of parameters for semiempirical methods V: modification of NDDO approximations and application to 70 elements. *Journal of Molecular Modeling*, *13*(12), 1173-1213.

Thiel, W. (2000). Semiempirical methods. *Modern Methods and Algorithms in Quantum Chemistry*, *3*, 261-283.

Thiel W. (2005). Semiempirical quantum-chemical methods in computational chemistry. *Elsevier B. V., 21*, 559-580.

Technology Transfer Network Air Toxics. (2016). Retrieved from U.S. Environmental Protection Agency (EPA): https://www3.epa.gov/ttn/atw/hlthef/hydrazin.html

Ultraviolet-Visible Spectra (UV). (2009). *Royal Society of Chemistry*. Retrieved from https://www.rsc.org

Varela-Álvarez, A., Sordo, J. A., & Scuseria, G. E. (2005). Doping of polyaniline by acid base chemistry: Density functional calculations with periodic boundary conditions. *Journal of the American Chemical Society*, *127*(32), 11318–11327.

Varela-Álvarez, A., & Sordo, J. A. (2008). A suitable model for emeraldine salt. *Journal of Chemical Physics*, *128*(17).

Wring, S. A., & Hart, J. P. (1992). Chemically modified, carbon-based electrodes and their application as electrochemical sensors for the analysis of biologically important compounds. A review. *Analyst*, *117*(8), 1215-1229.

Zhekova, H., Tadjer, A., Ivanova, A., Petrova, J., & Gospodinova, N. (2007). Theoretical study of the structure and electronic spectra of fully protonated emeraldine oligomers. *International Journal of Quantum Chemistry*, *107*(8), 1688-1706.

LIST OF PUBLICATIONS AND PAPER PRESENTED

Sabri F. N., Monajemi H., Zain S. M., Wai P. S., Rungrotmongkol T., & Lee V. S. (2016). Molecular conformation and UV–visible absorption spectrum of emeraldine salt polyaniline as a hydrazine sensor. *Integrated Ferroelectrics*, 175(1), 202-210.

Appendix A- Example of input files for ES-PANI, TD-DFT, ES-PANI 4+ charges

Monomer ES-PANI input file structure for optimisation calculation:

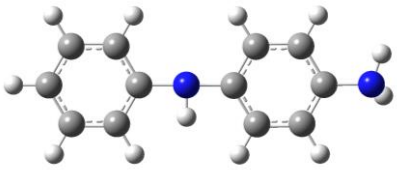

Monomer ES-PANI gaussian optimisation calculation input file:

%nprocshared=16

%mem=2GB

%rwf=2r_tilt.rwf

%nosave

%chk=C:\Users\USER\Desktop\opt_tilt\2r_tilt.chk

opt b3lyp/6-31g(d,p)

Title Card Required

1 2

C	-3.27825175	0.39211744	-0.32215467
C	-1.88309175	0.39211744	-0.32215467
C	-1.18555375	1.59986844	-0.32215467
C	-1.88320775	2.80837744	-0.32335367
C	-3.27803275	2.80829944	-0.32383267
C	-3.97563375	1.60009344	-0.32283667
H	-3.82801075	-0.56019956	-0.32170467
H	-1.33358375	-0.56039556	-0.32083967
H	-1.33300775	3.76052044	-0.32341267

H	-3.82815475	3.76058044	-0.32478567
H	-5.07523775	1.60027644	-0.32301667
N	0.28444600	1.59997538	-0.32130717
H	0.28451837	0.59997559	-0.32064785
C	1.75391548	1.57992962	-0.35533087
C	2.44330050	2.79274954	-0.37228803
C	2.45938349	0.37666132	-0.35823386
C	3.83782934	2.80219990	-0.39282494
H	1.88682013	3.74120570	-0.37077133
C	3.85435360	0.38594717	-0.37778021
H	1.91620214	-0.57931966	-0.34469082
C	4.54363385	1.59843463	-0.39521302
H	4.38127019	3.75811440	-0.40682548
H	4.41032359	-0.56293012	-0.37964908
N	6.01343955	1.60872975	-0.41678152
H	6.34003524	2.55382978	-0.42779019
H	6.33807278	1.13815888	-1.23725475

Tetramer ES-PANI with +1 charge input file structure for TD-DFT calculation:

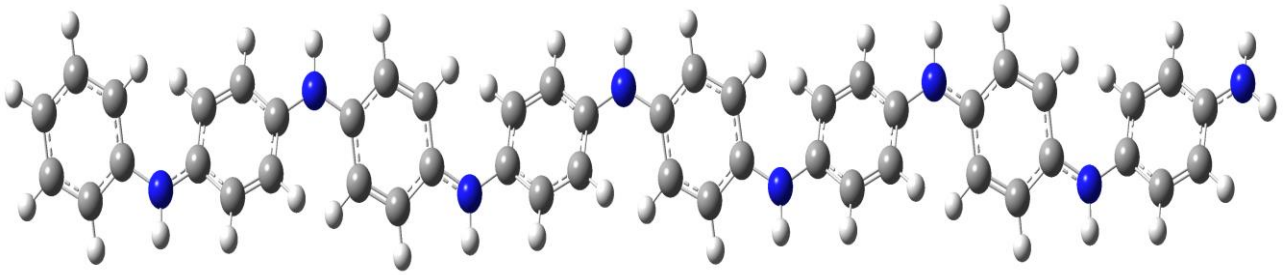

Tetramer ES-PANI with +1 charge input file for gaussian TD-DFT calculation:

%nprocshared=4

%mem=2GB

%rwf=8r_1ctdb3lyp.rwf

%nosave

%chk=C:\Users\USER\Desktop\master research\7_reduced charge\reduced charge_td\8r_1ctdb3lyp.chk

td=(nstates=10) ub3lyp/6-31g(d,p) scf=qc formcheck

Title Card Required

1 2

C	19.45031700	0.64787000	-0.87478900
C	18.17402600	1.18891500	-0.75167000
C	17.14213300	0.45076400	-0.14733600
C	17.42122900	-0.83826900	0.33692500
C	18.69906000	-1.37552300	0.19168300
C	19.72065400	-0.64205800	-0.41324400
H	20.23426500	1.23517000	-1.34349300
H	17.96519000	2.18631500	-1.13037100
H	16.65182400	-1.40337800	0.85012200

H	18.89902100	-2.37249300	0.57333000
H	20.71390300	-1.06614000	-0.51799800
N	15.88550700	1.05903300	0.00068000
H	15.89868500	2.06732700	0.04163800
C	14.62495100	0.47631300	0.06834700
C	14.34306400	-0.81576000	-0.41712700
C	13.55968700	1.22313900	0.60881900
C	13.05359100	-1.32466100	-0.35953400
H	15.12839800	-1.40737600	-0.87111700
C	12.27187100	0.71054000	0.66981200
H	13.75647700	2.21274900	1.01294200
C	11.99284100	-0.57739700	0.18010900
H	12.85667600	-2.31501100	-0.76208200
H	11.48898200	1.29739300	1.13590600
N	10.72318900	-1.16812000	0.25986100
H	10.72148600	-2.17541600	0.32870800
C	9.23326100	0.72712500	-0.24224700
C	7.95028000	1.25151600	-0.25626600
C	6.84833100	0.51422300	0.21536300
C	7.08279600	-0.78244900	0.71052100
C	8.36435500	-1.30980100	0.72212400
C	9.46988400	-0.57231600	0.25089100
H	10.05034400	1.30996400	-0.64909100
H	7.78928000	2.24598400	-0.66447600
H	6.26703300	-1.36287000	1.12460700
H	8.52476700	-2.30411200	1.13080200

N	5.58843000	1.11895100	0.21949700
H	5.59723100	2.12828900	0.24955000
C	4.32477300	0.53844900	0.18884700
C	4.08072000	-0.75777600	-0.30689400
C	3.22172700	1.29330300	0.63460800
C	2.79124600	-1.26420700	-0.34642300
H	4.89687600	-1.35249500	-0.69841500
C	1.93270400	0.78539200	0.59652100
H	3.38808200	2.28588700	1.04503800
C	1.68951200	-0.50953300	0.09974900
H	2.62468200	-2.25688600	-0.75663900
H	1.11754500	1.37918800	0.99183300
N	0.42363800	-1.09533500	0.07385300
H	0.41926300	-2.10516200	0.07825900
C	-1.06315900	0.80470700	-0.43653900
C	-2.34724600	1.32498400	-0.47559500
C	-3.45890600	0.57545000	-0.04484500
C	-3.23091300	-0.72860900	0.43600900
C	-1.94701400	-1.24891200	0.47518700
C	-0.83482700	-0.49924300	0.04489600
H	-0.24000400	1.39566100	-0.81897400
H	-2.50193400	2.32412300	-0.87449200
H	-4.05438000	-1.31943400	0.81820900
H	-1.79244600	-2.24806400	0.87412600
N	-4.71835400	1.17150000	-0.07095500
H	-4.71527200	2.18134900	-0.06091100

C	-5.98191400	0.58386700	-0.10728500
C	-6.21952500	-0.70747700	-0.61738900
C	-7.08777900	1.33084500	0.34282000
C	-7.50630600	-1.21849600	-0.66509000
H	-5.40072700	-1.29504600	-1.01452400
C	-8.37529500	0.82127500	0.29414500
H	-6.92543300	2.31959600	0.76402300
C	-8.61395400	-0.47103000	-0.21584300
H	-7.66825600	-2.20753200	-1.08575800
H	-9.19411700	1.40917700	0.68999000
N	-9.87384100	-1.05517800	-0.25958700
H	-9.87701600	-2.06370000	-0.31438400
C	-11.38849900	0.84674500	-0.68810300
C	-12.67344700	1.36468200	-0.67044700
C	-13.76881300	0.60645800	-0.20488200
C	-13.51674500	-0.70670400	0.24594600
C	-12.23010300	-1.21998400	0.23226000
C	-11.13844700	-0.46026000	-0.22860300
H	-10.58243500	1.44374400	-1.09758500
H	-12.84589500	2.36854000	-1.04982000
H	-14.32690000	-1.30861400	0.63875300
H	-12.05728500	-2.22479000	0.60929400
N	-15.02496500	1.18684000	-0.18305500
H	-15.04038700	2.19370500	-0.25678800
C	-16.28254800	0.56909700	-0.03936100
C	-16.58090400	-0.67979300	-0.60845300

C	-17.30361600	1.25189700	0.64047600
C	-17.84634100	-1.23604800	-0.47310600
H	-15.82712700	-1.20649900	-1.18310300
C	-18.57442600	0.70669900	0.75794800
H	-17.09384000	2.22053300	1.08663200
C	-18.87043900	-0.55681300	0.21265500
H	-18.05367100	-2.20462500	-0.92015900
H	-19.34576100	1.25470800	1.29205700
N	-20.11840800	-1.13697900	0.38978600
H	-20.37290400	-1.86340200	-0.26401300
H	-20.88166600	-0.50816200	0.59428700

Tetramer ES-PANI with +4 charge input file structure for optimisation calculation:

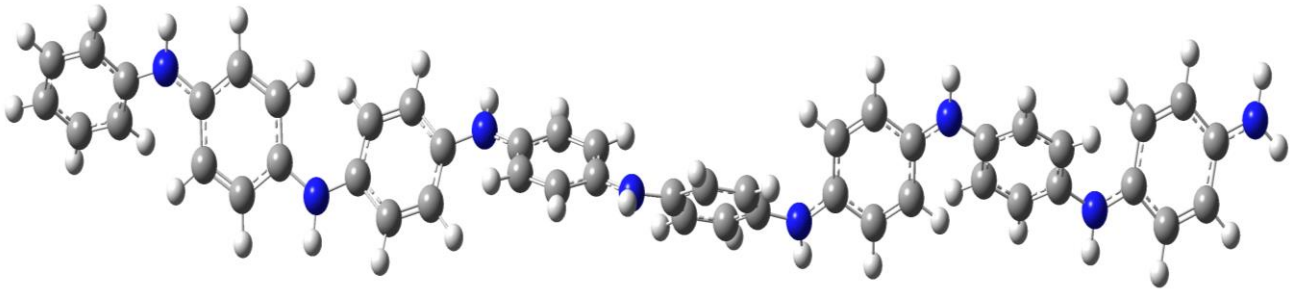

Tetramer ES-PANI with +4 charge for gaussian optimisation calculation input file:

%nprocshared=4

%mem=4GB

%rwf=tetramer_opt_050816.rwf

%nosave

%chk=C:\Users\USER\Desktop\opt after scan\tetramer_opt_050816.chk

opt ub3lyp/6-31g(d,p) scf=qc geom=connectivity

Title Card Required

4 5

C	19.34007900	0.87273500	-0.14610700
C	18.07829700	1.43303900	-0.05470900
C	16.92532300	0.59008400	0.14914900
C	17.13569100	-0.82218000	0.30435900
C	18.41406100	-1.34758700	0.21138400
C	19.52296100	-0.51655700	-0.02419000
H	20.21629400	1.52489300	-0.31630900
H	17.95794800	2.52542200	-0.15483600
H	16.29105700	-1.48606300	0.55189300

H	18.56700700	-2.43445500	0.33788700
H	20.53517800	-0.95050000	-0.10103300
N	15.69296500	1.17832300	0.22617900
H	15.67779500	2.18095700	0.35284900
C	14.44281800	0.56243300	0.16318700
C	14.21377300	-0.64433500	-0.55341600
C	13.33226600	1.19577300	0.79747900
C	12.94961400	-1.21134300	-0.59349200
H	15.02943800	-1.12119900	-1.12528600
C	12.07301700	0.61915800	0.75955300
H	13.46882100	2.14025100	1.35268200
C	11.84914700	-0.60109000	0.06953300
H	12.80741900	-2.14835700	-1.16016100
H	11.24321600	1.11469500	1.29179100
N	10.61395400	-1.25374300	0.08340300
H	10.63564800	-2.25212500	0.07339100
C	9.15263900	0.68435200	-0.35669500
C	7.88428500	1.23313800	-0.38421900
C	6.74642500	0.47151700	0.02355600
C	6.96211100	-0.85063600	0.50264900
C	8.23376900	-1.39255200	0.53357600
C	9.36828600	-0.64562200	0.09895300
H	10.00442700	1.29042800	-0.71042000
H	7.76099700	2.26673200	-0.75208000
H	6.12299400	-1.44369100	0.90505300
H	8.36294000	-2.41971000	0.91762000

N	5.49208500	1.07376700	-0.01435400
H	5.49629600	2.08227200	0.03046300
C	4.26451500	0.47701400	-0.12076500
C	4.07303300	-0.88267200	-0.52990000
C	3.08562000	1.25728000	0.15044400
C	2.81409000	-1.42599600	-0.61990700
H	4.94155900	-1.49636700	-0.82800000
C	1.82992400	0.70717600	0.06082700
H	3.18487200	2.31406800	0.45657200
C	1.64107000	-0.65695900	-0.32137300
H	2.71070900	-2.47599700	-0.94769000
H	0.95125200	1.33105300	0.30127700
N	0.40803500	-1.25444100	-0.39526300
H	0.37506800	-2.24711400	-0.50499900
C	-1.14243900	0.55986400	-1.02442800
C	-2.40698600	1.13368300	-0.95719800
C	-3.41976500	0.55478500	-0.15079400
C	-3.11187300	-0.59991400	0.60520300
C	-1.84391900	-1.16803300	0.54039700
C	-0.83739800	-0.60324100	-0.28012600
H	-0.38323900	1.01722600	-1.68139300
H	-2.61184200	2.03849000	-1.55465800
H	-3.86198700	-1.04801300	1.27837500
H	-1.63405800	-2.06753000	1.14440500
N	-4.67891800	1.18888800	-0.08033600
H	-4.65361900	2.19334000	-0.08680700

C	-5.89783900	0.59130300	-0.04410600
C	-6.10090600	-0.82003200	-0.23113500
C	-7.07541900	1.39803900	0.17442900
C	-7.35002300	-1.37013700	-0.19673000
H	-5.23056000	-1.46942400	-0.43654300
C	-8.32443600	0.84783500	0.20884800
H	-6.96466000	2.48655100	0.33340300
C	-8.52743300	-0.56346400	0.02184400
H	-7.46109800	-2.45862700	-0.35584600
H	-9.19490900	1.49738500	0.41366800
N	-9.74673800	-1.16060300	0.05794000
H	-9.77371600	-2.16500400	0.06318600
C	-11.31217200	0.62719000	-0.63205700
C	-12.58006600	1.19675900	-0.56885200
C	-13.58327600	0.63518600	0.25566500
C	-13.28076200	-0.52349000	1.00563400
C	-12.01584200	-1.09787900	0.94061000
C	-11.00500700	-0.52401300	0.12900000
H	-10.56262200	1.07186800	-1.30818500
H	-12.79065100	2.09276600	-1.17835900
H	-14.03909100	-0.97676200	1.66732500
H	-11.81159300	-2.00037400	1.54215900
N	-14.83753600	1.28126800	0.36070900
H	-14.80683800	2.27134300	0.50656600
C	-16.05715000	0.69263500	0.19314500
C	-16.22469500	-0.68778900	-0.16437500

C	-17.25119600	1.48213100	0.37116700
C	-17.46508800	-1.24004300	-0.31971000
H	-15.32990800	-1.31445900	-0.32924400
C	-18.49432700	0.93925900	0.22198200
H	-17.16143200	2.55139800	0.63956300
C	-18.66407800	-0.45379700	-0.12975300
H	-17.55799000	-2.30498500	-0.60037000
H	-19.38896000	1.57210100	0.37180900
N	-19.88396200	-0.99151100	-0.27604300
H	-19.99740800	-1.95395100	-0.52095200
H	-20.70828300	-0.44021900	-0.14561500

Tetramer ES-PANI with +4 charge input file structure for TD-DFT calculation:

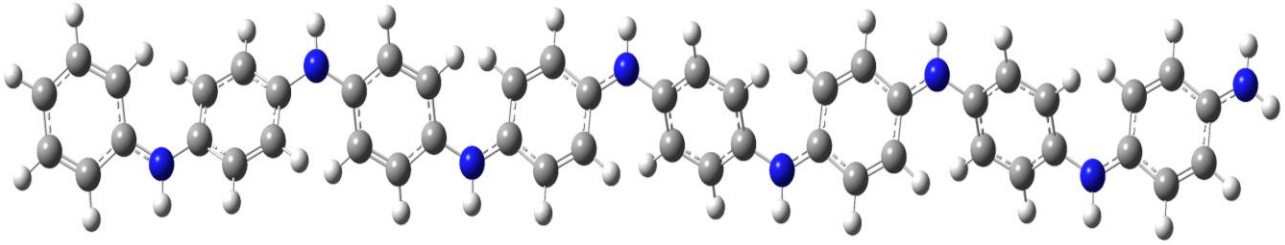

Tetramer ES-PANI with +4 charge for gaussian TD-DFT calculation input file:

%nprocshared=4

%mem=4GB

%rwf=8r_td_a.rwf

%nosave

%chk=C:\Users\USER\Desktop\cs_all\180316_td\8r_td_a.chk

td=(nstates=10) ub3lyp/6-31g(d,p) scf=qc

Title Card Required

4 5

C	19.34006700	0.87321500	-0.14643900
C	18.07825100	1.43344600	-0.05505600
C	16.92532100	0.59043100	0.14884800
C	17.13578000	-0.82181800	0.30410500
C	18.41418100	-1.34715200	0.21113800
C	19.52303400	-0.51606400	-0.02447100
H	20.21624400	1.52541900	-0.31666600
H	17.95783600	2.52581900	-0.15522000
H	16.29118700	-1.48574400	0.55166800
H	18.56719500	-2.43400600	0.33768200

H	20.53527800	-0.94995000	-0.10130200
N	15.69293500	1.17859700	0.22585500
H	15.67769500	2.18124500	0.35242200
C	14.44282000	0.56261700	0.16298500
C	14.21381300	-0.64418700	-0.55355700
C	13.33227800	1.19590600	0.79733100
C	12.94968600	-1.21127800	-0.59353000
H	15.02947300	-1.12101100	-1.12546700
C	12.07306100	0.61921100	0.75951300
H	13.46881000	2.14042000	1.35248000
C	11.84922300	-0.60107100	0.06954600
H	12.80751500	-2.14831700	-1.16016600
H	11.24326300	1.11472000	1.29178300
N	10.61405600	-1.25379000	0.08351400
H	10.63580400	-2.25217200	0.07356200
C	9.15263300	0.68422700	-0.35656000
C	7.88425700	1.23295300	-0.38405100
C	6.74644400	0.47129500	0.02377500
C	6.96220600	-0.85083900	0.50288700
C	8.23388400	-1.39270000	0.53377400
C	9.36836100	-0.64572800	0.09910300
H	10.00438300	1.29033700	-0.71032200
H	7.76090800	2.26653700	-0.75191700
H	6.12312700	-1.44390500	0.90535400
H	8.36311400	-2.41984300	0.91784200
N	5.49208600	1.07349700	-0.01410500

H	5.49626200	2.08200400	0.03069100
C	4.26452400	0.47671400	-0.12042600
C	4.07304200	-0.88297600	-0.52952000
C	3.08564500	1.25698000	0.15081300
C	2.81409500	-1.42630200	-0.61950300
H	4.94155400	-1.49667800	-0.82763800
C	1.82994400	0.70688500	0.06120600
H	3.18490600	2.31376700	0.45693700
C	1.64107700	-0.65725500	-0.32099400
H	2.71072300	-2.47630800	-0.94727000
H	0.95128300	1.33077600	0.30166000
N	0.40802600	-1.25471900	-0.39492600
H	0.37503700	-2.24738300	-0.50474300
C	-1.14241300	0.55961100	-1.02411200
C	-2.40695800	1.13343800	-0.95690900
C	-3.41975500	0.55453800	-0.15054000
C	-3.11187700	-0.60014600	0.60549300
C	-1.84393000	-1.16827300	0.54071000
C	-0.83739600	-0.60349800	-0.27980800
H	-0.38319600	1.01697800	-1.68105700
H	-2.61179400	2.03825100	-1.55436600
H	-3.86200500	-1.04821300	1.27867200
H	-1.63408000	-2.06777600	1.14471600
N	-4.67889600	1.18864800	-0.08005300
H	-4.65360500	2.19310200	-0.08668700
C	-5.89783100	0.59107800	-0.04405700

C	-6.10088600	-0.82026400	-0.23108200
C	-7.07542800	1.39781100	0.17435200
C	-7.35001100	-1.37035000	-0.19690200
H	-5.23049800	-1.46964900	-0.43632200
C	-8.32446500	0.84760800	0.20864300
H	-6.96469300	2.48632900	0.33332900
C	-8.52745000	-0.56366800	0.02150900
H	-7.46110800	-2.45883300	-0.35605000
H	-9.19493800	1.49716200	0.41345200
N	-9.74678000	-1.16076500	0.05739700
H	-9.77376700	-2.16516900	0.06241700
C	-11.31212300	0.62710200	-0.63245100
C	-12.57999700	1.19674400	-0.56921400
C	-13.58323500	0.63516500	0.25529600
C	-13.28077500	-0.52360800	1.00514800
C	-12.01590100	-1.09810000	0.94003700
C	-11.00501800	-0.52417200	0.12852500
H	-10.56254300	1.07176300	-1.30858200
H	-12.79056100	2.09276100	-1.17873200
H	-14.03912000	-0.97690000	1.66682600
H	-11.81172900	-2.00071600	1.54143100
N	-14.83744300	1.28136000	0.36048300
H	-14.80660100	2.27145200	0.50623000
C	-16.05715500	0.69288500	0.19301400
C	-16.22494700	-0.68748600	-0.16459500
C	-17.25106500	1.48253900	0.37128100

C	-17.46544800	-1.23956000	-0.31978700
H	-15.33028300	-1.31429800	-0.32962100
C	-18.49428500	0.93984900	0.22227600
H	-17.16108400	2.55176100	0.63978300
C	-18.66429400	-0.45316800	-0.12954600
H	-17.55852500	-2.30447800	-0.60050700
H	-19.38881200	1.57278100	0.37236900
N	-19.88428700	-0.99070500	-0.27562800
H	-19.99791500	-1.95310700	-0.52063400
H	-20.70850600	-0.43930600	-0.14498100

Appendix A- Example of output files for charge distribution with different charges assign on Tetramer ES-PANI

Charge distribution on Tetramer ES-PANI with +1 charge assigned:

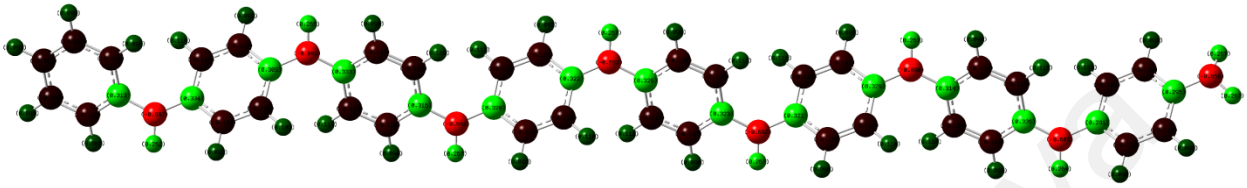

Mulliken atomic charges:

	1				
1	C	-0.087344	17 C	-0.136715	33 H 0.094040
2	C	-0.125281	18 H	0.113673	34 H 0.108622
3	C	0.312825	19 C	-0.108596	35 H 0.093690
4	C	-0.109604	20 H	0.091130	36 N -0.691987
5	C	-0.096425	21 C	0.309230	37 H 0.266707
6	C	-0.086202	22 H	0.091888	38 C 0.327798
7	H	0.096268	23 H	0.105295	39 C -0.111356
8	H	0.083421	24 N	-0.693405	40 C -0.140917
9	H	0.098568	25 H	0.265404	41 C -0.139443
10	H	0.094618	26 C	-0.113155	42 H 0.112788
11	H	0.093357	27 C	-0.138035	43 C -0.110138
12	N	-0.696838	28 C	0.316238	44 H 0.095078
13	H	0.262205	29 C	-0.109034	45 C 0.321884
14	C	0.334116	30 C	-0.142565	46 H 0.095221
15	C	-0.113513	31 C	0.333485	47 H 0.110353
16	C	-0.143224	32 H	0.112925	48 N -0.693043

49	H	0.267093	74	C	-0.108403
50	C	-0.110989	75	C	-0.143371
51	C	-0.139660	76	C	0.335700
52	C	0.323334	77	C	-0.114615
53	C	-0.110250	78	C	-0.136981
54	C	-0.140369	79	C	0.314386
55	C	0.325878	80	H	0.108107
56	H	0.111826	81	H	0.092886
57	H	0.095735	82	H	0.115198
58	H	0.111959	83	H	0.094377
59	H	0.095626	84	N	-0.689257
60	N	-0.691579	85	H	0.264477
61	H	0.267493	86	C	0.290737
62	C	0.322036	87	C	-0.106774
63	C	-0.109824	88	C	-0.122392
64	C	-0.139386	89	C	-0.124460
65	C	-0.140919	90	H	0.103158
66	H	0.110999	91	C	-0.116384
67	C	-0.111087	92	H	0.089927
68	H	0.095759	93	C	0.294752
69	C	0.329241	94	H	0.087764
70	H	0.095685	95	H	0.089988
71	H	0.113566	96	N	-0.656300
72	N	-0.690059	97	H	0.266670
73	H	0.267484	98	H	0.267211

Charge distribution on Tetramer ES-PANI with +2 charge assigned:

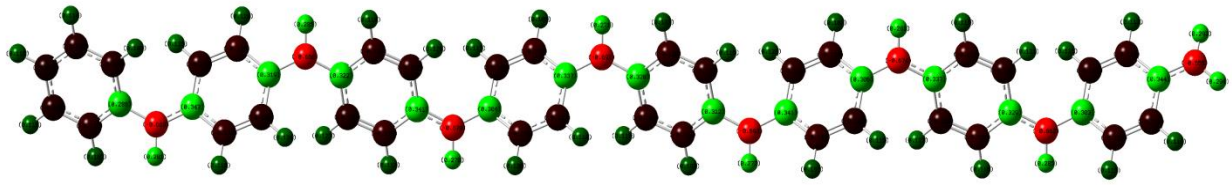

Mulliken atomic charges:

	1				
1	C	-0.086388	19 C	-0.100523	37 H 0.278495
2	C	-0.111953	20 H	0.115038	38 C 0.303978
3	C	0.288300	21 C	0.319485	39 C -0.103336
4	C	-0.100404	22 H	0.115188	40 C -0.130431
5	C	-0.094911	23 H	0.123718	41 C -0.141261
6	C	-0.075146	24 N	-0.665683	42 H 0.117003
7	H	0.117641	25 H	0.284598	43 C -0.112292
8	H	0.102034	26 C	-0.100583	44 H 0.106312
9	H	0.108882	27 C	-0.138438	45 C 0.337466
10	H	0.114011	28 C	0.340555	46 H 0.104879
11	H	0.116471	29 C	-0.106866	47 H 0.117868
12	N	-0.669245	30 C	-0.132210	48 N -0.696764
13	H	0.280829	31 C	0.322297	49 H 0.270946
14	C	0.346637	32 H	0.126879	50 C -0.109319
15	C	-0.104419	33 H	0.113113	51 C -0.133746
16	C	-0.137010	34 H	0.125693	52 C 0.312032
17	C	-0.131545	35 H	0.114370	53 C -0.107322
18	H	0.134659	36 N	-0.678970	54 C -0.136268

55	C	0.319561	80	H	0.126875
56	H	0.114922	81	H	0.116042
57	H	0.103192	82	H	0.130654
58	H	0.114645	83	H	0.115224
59	H	0.102882	84	N	-0.662126
60	N	-0.693194	85	H	0.284574
61	H	0.272375	86	C	0.302886
62	C	0.341021	87	C	-0.100570
63	C	-0.111901	88	C	-0.119157
64	C	-0.141521	89	C	-0.123511
65	C	-0.130252	90	H	0.120779
66	H	0.119923	91	C	-0.112008
67	C	-0.102275	92	H	0.113218
68	H	0.106769	93	C	0.344148
69	C	0.305575	94	H	0.111967
70	H	0.108295	95	H	0.115938
71	H	0.119056	96	N	-0.654914
72	N	-0.673728	97	H	0.293208
73	H	0.280909	98	H	0.294326
74	C	-0.104556			
75	C	-0.133035			
76	C	0.329448			
77	C	-0.100961			
78	C	-0.136516			
79	C	0.337467			

Charge distribution on Tetramer ES-PANI with +3 charge assigned:

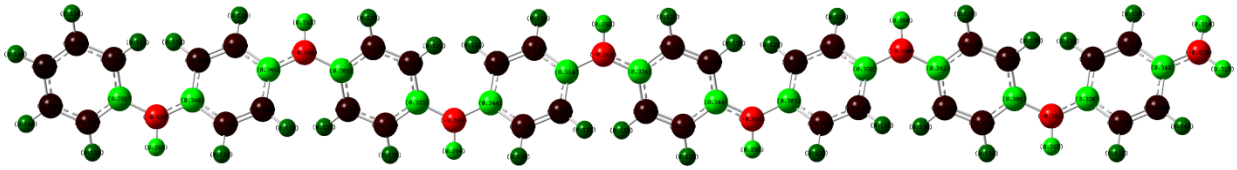

Mulliken atomic charges:

	1								
1	C	-0.082072	19	C	-0.098661	37	H	0.284425
2	C	-0.107234	20	H	0.134939	38	C	0.343504
3	C	0.291464	21	C	0.346305	39	C	-0.105625
4	C	-0.094322	22	H	0.133151	40	C	-0.136439
5	C	-0.092156	23	H	0.136999	41	C	-0.127250
6	C	-0.064136	24	N	-0.665740	42	H	0.130746
7	H	0.139799	25	H	0.292528	43	C	-0.097087
8	H	0.120839	26	C	-0.098876	44	H	0.123558
9	H	0.122441	27	C	-0.132070	45	C	0.314382
10	H	0.134479	28	C	0.325059	46	H	0.124049
11	H	0.140471	29	C	-0.105167	47	H	0.130890
12	N	-0.639150	30	C	-0.124428	48	N	-0.661255
13	H	0.298667	31	C	0.303242	49	H	0.292298
14	C	0.340466	32	H	0.132058	50	C	-0.096300
15	C	-0.089739	33	H	0.122970	51	C	-0.132582
16	C	-0.124261	34	H	0.128647	52	C	0.343671
17	C	-0.131416	35	H	0.124583	53	C	-0.099845
18	H	0.151559	36	N	-0.687668	54	C	-0.129466

55	C	0.333637	80	H	0.129601
56	H	0.135922	81	H	0.126791
57	H	0.127794	82	H	0.135864
58	H	0.136063	83	H	0.124589
59	H	0.127942	84	N	-0.650776
60	N	-0.669216	85	H	0.296529
61	H	0.289741	86	C	0.330024
62	C	0.306823	87	C	-0.093937
63	C	-0.099874	88	C	-0.116349
64	C	-0.126643	89	C	-0.109787
65	C	-0.133519	90	H	0.138383
66	H	0.128081	91	C	-0.097831
67	C	-0.105450	92	H	0.135226
68	H	0.122120	93	C	0.348864
69	C	0.330128	94	H	0.136261
70	H	0.121863	95	H	0.141509
71	H	0.129392	96	N	-0.624799
72	N	-0.690096	97	H	0.313781
73	H	0.283833	98	H	0.315413
74	C	-0.106556			
75	C	-0.124473			
76	C	0.308024			
77	C	-0.095476			
78	C	-0.136805			
79	C	0.342145			

Charge distribution on Tetramer ES-PANI with +4 charge assigned:

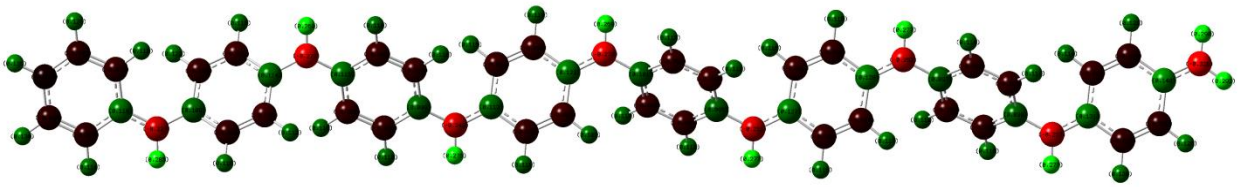

Mulliken atomic charges:

	1				
1	C	-0.047821	19 C	-0.065305	37 H 0.275474
2	C	-0.050987	20 H	0.115504	38 C 0.111922
3	C	0.117554	21 C	0.114270	39 C -0.061513
4	C	-0.057201	22 H	0.115246	40 C -0.058303
5	C	-0.049914	23 H	0.112495	41 C -0.065045
6	C	-0.023148	24 N	-0.272774	42 H 0.114534
7	H	0.130346	25 H	0.268755	43 C -0.068838
8	H	0.114281	26 C	-0.068448	44 H 0.110696
9	H	0.110472	27 C	-0.060024	45 C 0.122789
10	H	0.125508	28 C	0.098714	46 H 0.110406
11	H	0.134965	29 C	-0.063578	47 H 0.109280
12	N	-0.226504	30 C	-0.066186	48 N -0.269968
13	H	0.285362	31 C	0.115139	49 H 0.269039
14	C	0.104640	32 H	0.110282	50 C -0.063823
15	C	-0.056090	33 H	0.109770	51 C -0.062341
16	C	-0.055903	34 H	0.110435	52 C 0.095131
17	C	-0.063010	35 H	0.110023	53 C -0.064783
18	H	0.121625	36 N	-0.243118	54 C -0.063342

55	C	0.100967	80	H	0.111962
56	H	0.113234	81	H	0.116262
57	H	0.111966	82	H	0.117471
58	H	0.111001	83	H	0.114278
59	H	0.112909	84	N	-0.257301
60	N	-0.250637	85	H	0.277453
61	H	0.277004	86	C	0.130856
62	C	0.126817	87	C	-0.061462
63	C	-0.061489	88	C	-0.055817
64	C	-0.057812	89	C	-0.053576
65	C	-0.058199	90	H	0.113765
66	H	0.116298	91	C	-0.052465
67	C	-0.061709	92	H	0.119539
68	H	0.115055	93	C	0.147677
69	C	0.128291	94	H	0.121401
70	H	0.115190	95	H	0.126398
71	H	0.116951	96	N	-0.326207
72	N	-0.251937	97	H	0.289981
73	H	0.277416	98	H	0.292116
74	C	-0.064143			
75	C	-0.060416			
76	C	0.098980			
77	C	-0.060937			
78	C	-0.061160			
79	C	0.097336			